

Millimeter Wave Imaging Architecture for On-The-Move Whole Body Imaging

Borja Gonzalez-Valdes, *Member, IEEE*, Yuri Álvarez, *Senior Member, IEEE*,
Yolanda Rodriguez-Vaqueiro, *Student Member, IEEE*, Ana Arboleya-Arboleya,
Antonio García-Pino, *Senior Member, IEEE*, Carey M. Rappaport, *Fellow, IEEE*,
Fernando Las-Heras, *Senior Member, IEEE*, and Jose A. Martinez-Lorenzo, *Member, IEEE*

Abstract—This paper presents a novel interrogation system that combines multiple millimeter wave transmitters and receivers to create real-time high-resolution radar images for personnel security screening. The main novelty of the presented system is that the images can be created as the person being screened continuously moves across a corridor where the transmitters and receivers, working in a fully coherent architecture, are distributed. As the person moves, the transmitters and receivers are sequentially activated to collect data from different angles to inspect the whole body. Multiple images, similar to video frames, are created and examined to look for possible anomalies such as concealed threats. Two-dimensional (2-D) and three-dimensional (3-D) setups have been simulated to show the feasibility of the proposed system. The simulation results in 2-D have been validated using measurements.

Index Terms—Backpropagation imaging, checkpoint, fast Fourier transform (FFT), imaging systems, multistatic radar system.

I. INTRODUCTION

IN homeland security applications, there is an increasing demand for methods to improve personnel screening for concealed object and contraband detection at security checkpoints. In this context, active nearfield millimeter-wave (mm-wave) imaging radar systems are able to provide high-resolution imaging at an affordable cost. The object of interest is first illuminated by mm waves and then the scattered field is

Manuscript received June 18, 2015; revised January 11, 2016; accepted February 18, 2016. Date of publication XXXX XX, XXXX; date of current version XXXX XX, XXXX. This work was supported in part by the Ministerio de Ciencia e Innovación of Spain/FEDER under project MIRIEM-TEC2014-54005-P, in part by the Gobierno del Principado de Asturias through the PCTI 2013-2017, GRUPIN14-114, in part by the Spanish Government under project TACTICA, in part by the European Regional Development Fund (ERDF), in part by the Galician Regional Government under Projects CN2012/279, CN2012/260 (AtlantTIC) and the Plan I2C (2011–2015), and in part by the Science and Technology Directorate, U.S. Department of Homeland Security under the Award Number 2008-ST-061-ED0001.

B. Gonzalez-Valdes, Y. Rodriguez-Vaqueiro, and A. García-Pino are with the Atlantic Research Center, Universidad de Vigo, 36310 Vigo, Spain (e-mail: bgvaldes@com.uvigo.es; yrvaqueiro@com.uvigo.es; agpino@com.uvigo.es).

Y. Álvarez, A. Arboleya Arboleya, and F. Las-Heras are with the Area of Signal Theory and Communications, Department of Electrical Engineering, Universidad de Oviedo, E-33203 Gijón, Spain (e-mail: yalopez@tsc.uniovi.es; aarboleya@tsc.uniovi.es; flasheras@tsc.uniovi.es).

C. M. Rappaport and J. A. Martinez are with the ALERT Center, Northeastern University, Boston, MA 02115 USA (e-mail: rappaport@ece.neu.edu; jmartine@ece.neu.edu).

Color versions of one or more of the figures in this paper are available online at <http://ieeexplore.ieee.org>.

Digital Object Identifier 10.1109/TAP.2016.2539372

measured and processed to reconstruct the surface (or volume) of the object.

The development of checkpoints that allow high passenger flow is becoming a priority. This has motivated the design of mm-wave imaging systems that minimize passenger inconvenience.

The International Air Transport Association (IATA) has defined several specifications that future checkpoints for personnel screening should meet. Novel paradigms in the design of the checkpoints specify that “from 2020 and beyond it is envisaged that the passenger will be able to flow through the security checkpoint without interruption unless the advanced technology identifies a potential threat,” [1] (page 14).

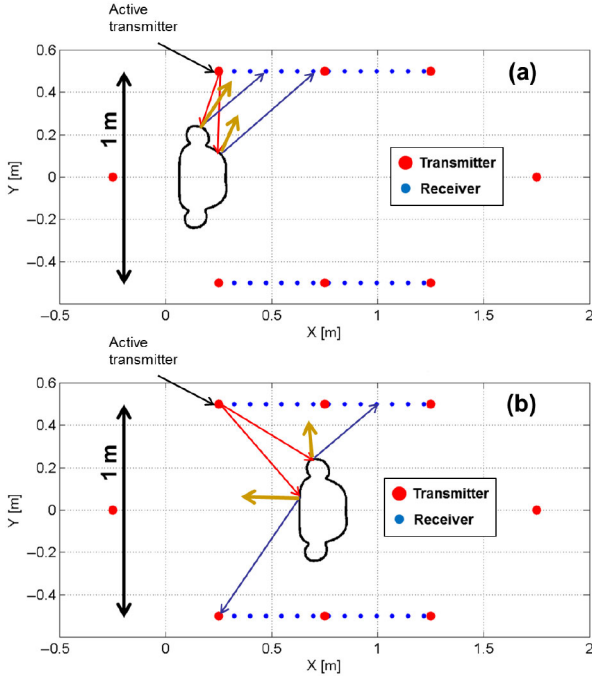
In [1], a computer graphics design of the checkpoint of the future proposed by IATA is presented. The novelty with respect to existing architectures is the inclusion of a beltway or hallway to avoid passenger flow interruption.

Current state-of-the-art mm-wave imaging systems for security screening require people to enter and stand in front of the scanning system. Mm-wave generation and acquisition can be achieved using static arrays of transmitters and receivers [2], [3], or using movable arrays to create planar [4], [5], or cylindrical [6]–[8] acquisition domains. Most of them are based on monostatic radar and Fourier inversion [2]–[6]. Monostatic imaging systems are cost effective, but they are only able to reconstruct surfaces that create specular reflection and they are not well suited for imaging scattering objects with sudden profile variations [9]. Further, they are prone to dihedral artifacts as described in [8], [10], and [11].

Based on the new checkpoint architecture proposed by the IATA, this paper introduces a novel concept for mm-wave scanning system for personnel screening. The proposed imaging system does not include any mechanical movement, and whole body imaging is obtained taking advantage of the movement of the person under test when passing through the system on a moving walkway.

The main contribution of this paper is the introduction of this novel architecture, called on-the-move imaging [12], [13], that, to the best of the author’s knowledge, has not been previously conceived nor demonstrated.

This paper is structured as follows. Section II describes the proposed mm-wave screening system. Imaging algorithm for multistatic setups is briefly described in Section III. Proof-of-concept is validated through two-dimensional (2-D) simulation



F1:1 Fig. 1. On-the-move imaging concept. OUT movement between the two walls
 F1:2 of radar antennas provides multiple points-of-view for every transmitter and
 F1:3 receiver, thus increasing multistatic information. (a) and (b) represent two
 F1:4 different OUT positions within the hallway.

76 examples in Section IV, and measurement results in Section V.
 77 Extension to two-dimensional (3-D) whole human body imag-
 78 ing is described and validated in Section VI. Finally, the
 79 conclusion is presented in Section VII.

80 II. ON-THE-MOVE HALLWAY CONCEPT

81 The novel mm-wave on-the-move imaging system for per-
 82 sonnel screening takes advantage of: 1) the movement of the
 83 person when passing through the imaging system and 2) a mul-
 84 tistatic radar configuration, where some of the transmitters and
 85 receivers are separated with a subtended angle relative to the
 86 person equal or greater than 90° to capture information from
 87 all possible wave incident and scattering angles.

88 A top view of the suggested multistatic architecture is plot-
 89 ted in Fig. 1. Several transmitters (red dots) and receivers (blue
 90 dots) are placed on the sides of the hallway. The person moves
 91 along the security checkpoint on a moving walkway.

92 The imaging radar system takes advantage of multiple inci-
 93 dence angles that illuminate different areas of the person
 94 depending on the active transmitter and the placement of the
 95 person within the hallway, as illustrated in Fig. 1. A single
 96 transmitter can illuminate different areas of the person while
 97 crossing the hallway. Reciprocally, the scattered field is col-
 98 lected by different receivers depending on the transmitting
 99 element and the current position of the person. This is illus-
 100 trated with the red and blue arrows in Fig. 1 that represent
 101 direct reflection contributions given by the incident angle and
 102 the normal to the surface according to Snell's law.

103 Multistatic information can be incremented by placing trans-
 104 mitters at the hallway ends. For practical implementation, this

TABLE I
 COMPARISON WITH STATE-OF-THE-ART MM-WAVE IMAGING SYSTEMS

Reference	Scanning area (cm) ¹	PSF (mm) ²	Frequency band (GHz)	Number of antennas
On-the-move	100×200^3	10×10	15 – 30	2×80601 Rx 60 Tx
UWB MIMO array, [5]	50×130	10×10	2.8 – 19.5	4 Tx 8 Rx, Height motion.
Flat 2-D array, [2]	100×200	3.0×1.5	72 – 80	3072 Tx 3072 Rx
Linear array, vertical movement [4]	72.6 Movable 2 m in height	10.0×3.8	27 – 33	66 Tx, 66 Rx, Height motion

¹Scanning area size: width \times height.

²PSF (point spread function): range \times cross range.

³Receiving panels size.

would partially block the persons path. This is solved in the 3-D
 case placing the receivers at the hallway ends below and above
 the moving walkway.

For every transmitter, the scattered field is collected on the
 receiving arrays placed on the hallway sides, and for every
 receiving array, a reflectivity image is recovered. The reflectiv-
 ity images associated with each transmitter are coherently com-
 bined. This configuration assumes that, for a single position,
 the body remains still while all the transmitters are sequen-
 tially activated and the scattered field is collected by the receivers.
 In this sense, and since the acquisition on the receivers can be
 done in parallel, the use of a low number of transmitters is desir-
 able. A fully electronic scanning system similar to the one in [3]
 would easily allow for such an acquisition procedure.

A critical aspect in the design of the imaging system is the
 selection of the frequency band. Table I shows a comparison
 among the proposed hallway concept and some of the exist-
 ing mm-wave scanning systems. It can be observed that, for
 a given size of the scanner, higher frequency bands provide
 better cross-range resolution, at the expense of losing dynamic
 range due to free-space propagation losses. Furthermore, cloth-
 ing becomes less transparent for these higher frequency bands,
 and radiofrequency hardware becomes more expensive. The
 work presented in [5] addresses the aforementioned drawbacks
 introducing an ultra-wideband (UWB) imaging system. In addi-
 tion to the improved range resolution and dynamic range, the
 novelty of this study is the fact that the sampling rate can be
 relaxed by taking advantage of grating lobes cancellation in
 UWB arrays, which will be of interest concerning practical
 implementation of the on-the-move architecture.

III. IMAGING ALGORITHM

Practical mm-wave scanning system implementation
 demands real-time imaging capabilities. Standard backprop-
 agation techniques [14] require millions of calculations for
 electrically large acquisition and imaging domains. To illus-
 trate the numerical magnitude of the problem, typical values
 for acquisition points and imaging voxels are 10^5 and 10^7 ,

142 respectively, assuming an operational frequency of 30 GHz
 143 ($\lambda = 1$ cm) and sampling every half wavelength in both
 144 domains according to Nyquist criterion.

145 The reflectivity function on a volumetric domain
 146 $\rho_t(x', y', z')$ can be recovered from the scattered field
 147 $E_{scatt}^t(f, x, z)$ acquired on a flat receiving aperture placed at
 148 $y = Y_0$, by solving the following integral equation [9], [14],
 149 when the t th (with t from 1 to N_{tx}) of a group of transmitters
 150 is active

$$\begin{aligned} \rho_t(x', y', z') &= \iiint E_{scatt}^t(f, x, z) e^{+jk((x-x')^2 + (Y_0 - y')^2 + (z-z')^2)^{1/2}} \\ &e^{+jk((x_{inc}^t - x')^2 + (y_{inc}^t - y')^2 + (z_{inc}^t - z')^2)^{1/2}} df dx dz \end{aligned} \quad (1)$$

151 where $(x_{inc}^t, y_{inc}^t, z_{inc}^t)$ denotes the position of the t th point
 152 source-like transmitter, $k = 2\pi f/c$, y -axis is the range axis
 153 (depth), x - and z -axes are horizontal and vertical cross ranges,
 154 and f is the frequency.

155 Fast propagation techniques, such as the inverse fast multi-
 156 pole method, have been proposed [15], reducing the calculation
 157 time by several orders of magnitude. Moreover, (1) can be par-
 158 allelized taking advantage of GPU hardware. However, these
 159 solutions are still too computationally expensive for applica-
 160 tions requiring real-time imaging.

161 Fourier-based techniques have been widely used in mono-
 162 static setups for real-time imaging [3]–[5], thanks to the fact
 163 that plane wave incidence can be considered during the inver-
 164 sion. Multistatic setups require different Fourier processing as
 165 the transmitter and receiver are placed in different positions. A
 166 novel Fourier-based imaging technique, totally suitable for the
 167 proposed hallway-based on-the-move imaging system, is pre-
 168 sented in [9]. The idea is to decompose the imaging domain in
 169 smaller regions where an incident spherical wave can be locally
 170 treated as a plane wave. Imaging calculations for every region
 171 can be carried out in parallel, without jeopardizing the required
 172 real-time capabilities of the multistatic imaging system.

173 When multiple transmitters are used, the final reconstruc-
 174 tion for a certain voxel placed in (x', y', z') can be obtained
 175 by combining the images generated by each transmitter as

$$\rho(x', y', z') = \sum_{t=1}^{N_{tx}} \rho_t(x', y', z'). \quad (2)$$

176 This formulation assumes all the transmitters and receivers
 177 work in a fully coherent configuration using a clock signal that
 178 provides common phase reference.

179 IV. 2-D RESULTS

180 The proposed on-the-move imaging is first validated using a
 181 2-D example. The frequency band ranges from 15 to 30 GHz,
 182 sampled every 300-MHz frequency steps and providing 1-cm
 183 range resolution. Two 1-m width lateral arrays of receivers
 184 with 50 evenly spaced elements are placed at $Y_0 = -0.6$ m
 185 and $Y_0 = 0.6$ m. Five transmitters are interleaved among each

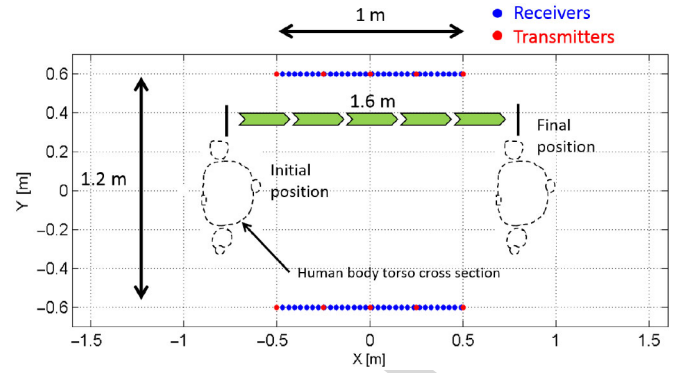


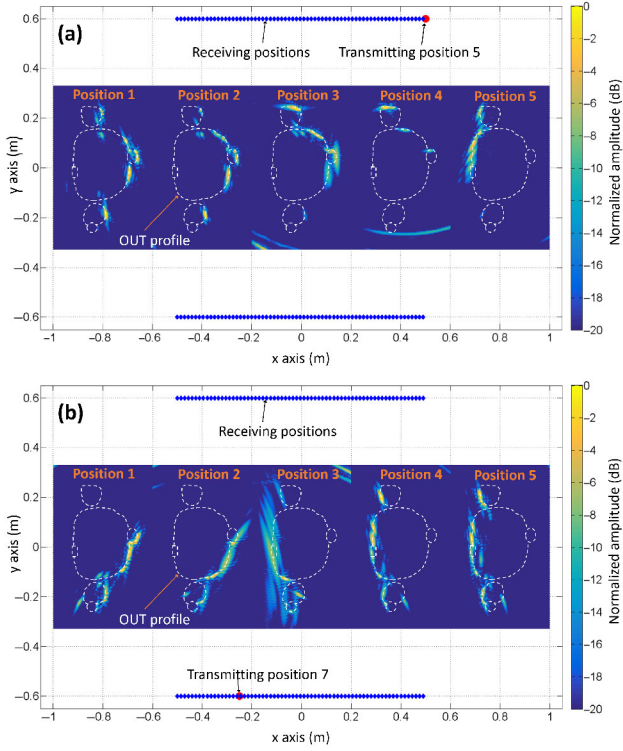
Fig. 2. 2-D example layout. OUT is displaced from position $x = -0.8$ m to $x = +0.8$ m, in five steps ($N_{pos} = 5$). 5 Tx and 50 Rx per side are considered.

panel of receivers, thus resulting in $N_{tx} = 10$ transmitters. The described layout is plotted in Fig. 2. The essential aspect is that, in order to image the entire body surface, for every transmitter, receivers on both walls must receive the scattered waves (not just those adjacent to a given transmitter.)

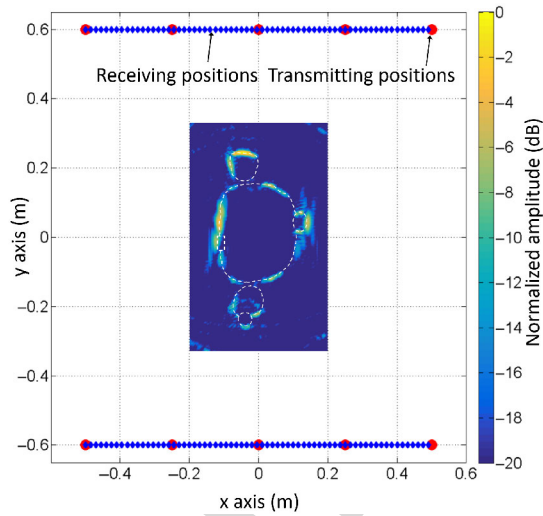
The object under test (OUT) models the cross section of a human body torso (for a more realistic simulation, arms and waist are not connected), with three attached objects on it represented as protrusions on the front, back, and arm. The object in the front is an elliptical cross-sectional metallic object. Dielectric objects ($\epsilon_r = 3.5$) are placed on the back (square cross section) and on the right arm. The OUT is displaced from the position $x = -0.8$ m to $x = 0.8$ m in 40-cm steps obtaining $N_{pos} = 5$ intermediate positions. For every position, the ten transmitters are sequentially activated and the scattered field is collected in the receiving points. A realistic composition of the human body tissue is considered [16], using a finite-difference frequency-domain (FDFD) code [17], [18] to calculate the scattered field for every transmitter and every OUT position. FDFD simulation results have confirmed that, due to the high conductivity of the skin in the frequency band of interest, the assumption that the OUT is a perfect electric conductor (PEC) is a good approximation for most cases.

The data are then used to create one reflectivity image for each intermediate position, ρ^p according to (1) and (2). The imaging domain is an $(X, Y) = (0.4, 0.6)$ m rectangle, discretized in 81×121 pixels and centered in (x'_p, y'_p, z'_p) . In this case, the computational cost is low and the image is recovered using the standard backpropagation algorithm in (1). For every p th OUT position and t th active transmitter, the image is recovered in about 1 s using a conventional laptop (2.5-GHZ CPU and 4-GB RAM memory). As the 2-D imaging code is not parallelized yet, it takes about 50 s for the entire reconstruction.

The obtained images for two different active transmitters when the OUT is in each of the intermediate positions are presented in Fig. 3. It is clear that each transmitter allows the reconstruction of different areas of the body depending on its relative position inside the imaging system. The image obtained for the central position, combining the images created using all the transmitters according to (2), is presented in Fig. 4.



F3:1 Fig. 3. Obtained images (normalized reflectivity amplitude in dB) for two dif-
 F3:2 ferent active transmitters and five intermediate positions using the setup in
 F3:3 Fig. 2. Active transmitters are depicted as red points. Blue points represent
 F3:4 receivers positions.



F4:1 Fig. 4. Obtained image when the OUTF is in the central position and the image
 F4:2 is created using all transmitters according to (2).

226 The reflectivity image created by the system at each position
 227 is obtained as

$$I(x'', y'', z'') = \sum_{p=1}^{N_{pos}} |\rho(x' - x'_p, y' - y'_p, z' - z'_p)| \quad (3)$$

228 where the reflectivity of all the positions is centered at the origin
 229 of coordinates before being combined. Absolute value is used
 230 since the position of the OUTF relative to the imaging system can
 231 slightly change from position to position, which prevents the

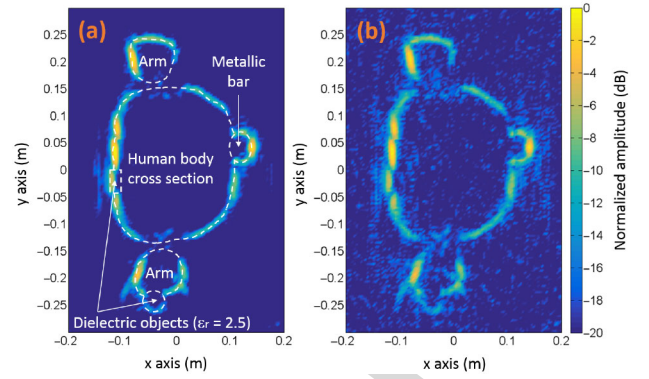


Fig. 5. Recovered OUTF profile when combining in amplitude the five images F5:1
 (one for each position). (a) SNR = 10 dB. (b) SNR = -20 dB. F5:2

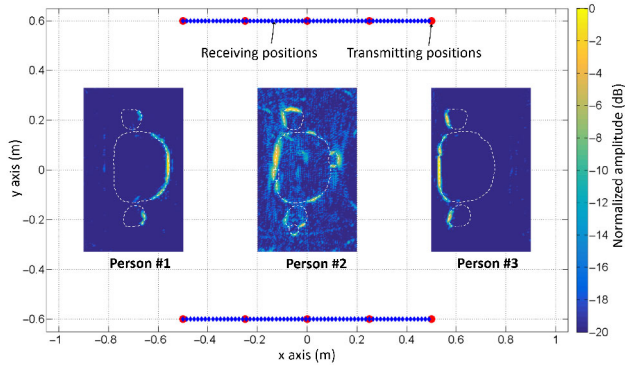
combination of the images of each position in amplitude and 232
 and phase. Fig. 5 presents the final result when the five analyzed 233
 positions are combined according to (3), and when the object 234
 retains exactly the same configuration for all positions and it is 235
 only displaced in the x direction. This proves the ability of the 236
 proposed system to obtain a complete contour reconstruction. 237
 In general, the images used for threat detection in a final 238
 configuration would be the ones generated in each position as the 239
 one in Fig. 4. 240

Combining the information from multiple transmitters and 241
 positions also helps to increase the dynamic range of the system. 242
 Sensitivity analysis has been performed: first, the recorded 243
 signal strength in the receiving arrays for every transmitting element 244
 and OUTF position has been evaluated. The case in which maximum 245
 power is recorded corresponds to the OUTF at the central position 246
 illuminated by the center transmitters. The minimum power levels 247
 are recorded for the OUTF in positions 1 or 248
 5 illuminated by the closest pair of transmitters, as only a small 249
 fraction of the scattered field is collected by the arrays. The 250
 received power difference between these two cases is 11 dB. 251

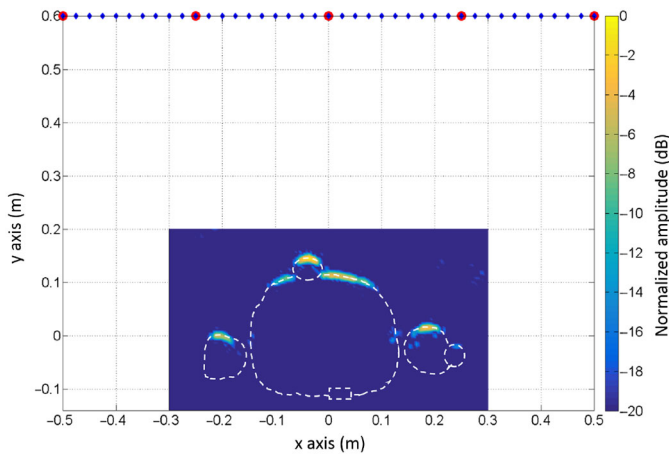
Next, noise has been added to the field samples according to 252
 different signal-to-noise ratio (SNR) levels relative to the maximum- 253
 recorded power case. Figs. 3–5(a) correspond to SNR = 10 dB, and 254
 Fig. 5(b) to SNR = -20 dB. Thanks to the combination of multiple 255
 OUTF positions and incident directions, the resulting mm-wave imaging 256
 system is able to work with low SNR. 257
 258

The capability of imaging multiple users within the hallway 259
 has been also evaluated. For this purpose, the OUTF placed at the 260
 center position (as in Fig. 4) is considered, but with two more 261
 OUTFs (with no attached objects) at $x = 0.7$ and $x = -0.7$ m, a 262
 scenario that could correspond to a high passenger throughput 263
 situation. Due to the use of FDFD simulations, multiple reflections 264
 among OUTFs are considered. Results are depicted in Fig. 6. It can 265
 be noticed that, with respect to Fig. 4, the center OUTF is worse 266
 imaged due to the multipath effects. It is also possible to create the 267
 image of the front and the back of the OUTFs placed at $x = 0.7$ and 268
 $x = -0.7$ m, and these results are not affected by multipath as 269
 much as the center OUTF. 270

In order to compare this work with current state of the art 271
 systems, Fig. 7 presents the obtained image when the same contour 272
 is facing a line containing the transmitters and receivers. In 273



F6:1 Fig. 6. Recovered image for three OUTs placed at the same time in the hallway.
 F6:2 The image is created by combining all transmitters according to (2).



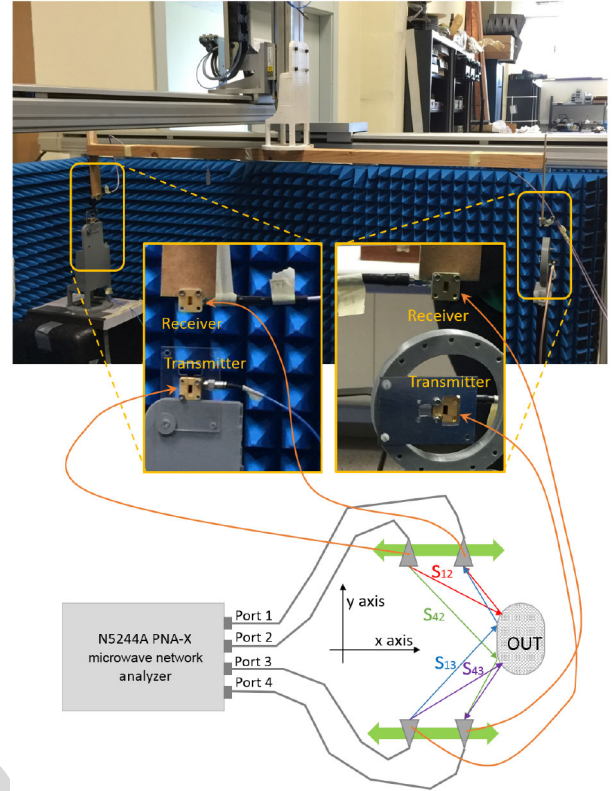
F7:1 Fig. 7. Obtained image using state-of-the-art configurations where transmitters
 F7:2 and receivers are placed in the same aperture and facing the person under test.
 F7:3 The image is generated combining the five transmitters according to (2).

274 this case, different areas of the front of the contour cannot be
 275 recovered and the area that is reconstructed is much smaller
 276 than the one of Fig. 4. Concerning detection capabilities, note
 277 that the dielectric object placed on the arm is hardly detected
 278 in Fig. 7 as the energy is not scattered back to the receiving
 279 array. In the case of the on-the-move system, it can be better
 280 detected (see Figs. 4 and 5), as it is possible to find a configura-
 281 tion along the conveyor belt in which the energy is reflected
 282 in the dielectric-skin transition, then backscattered to one of the
 283 receiving arrays.

284 This 2-D example proves that, in the proposed on-the-move
 285 layout, the fact that some of the transmitters and receivers are
 286 separated with a subtended angle relative to the person equal or
 287 greater than 90° provides information from all possible wave
 288 incident angles.

289 V. VALIDATION WITH MEASUREMENTS

290 The proposed on-the-move imaging concept has been vali-
 291 dated with measurements. Ka frequency band (26.5–40 GHz)
 292 has been selected to avoid hardware switching between differ-
 293 ent frequency bands. In order to ensure the maximum illumina-
 294 tion within the hallway, WR-28 open-ended waveguides are
 295 selected as antennas.

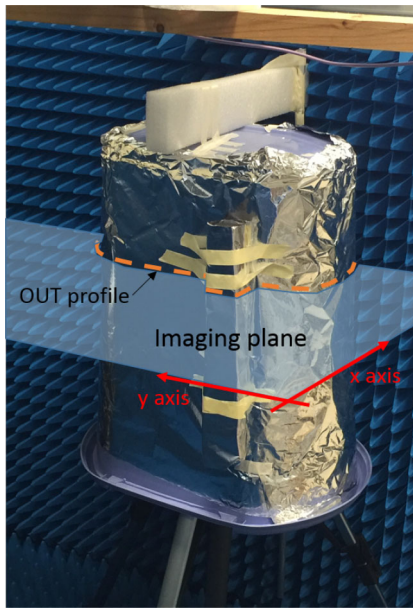


F8:1 Fig. 8. Ka-band measurement system for on-the-move concept experimental
 F8:2 validation. WR-28 open-ended waveguides are connected to the vector network
 F8:3 analyzer ports. Receivers are mounted on a three-axis positioner.

The setup is mounted on an XYZ table measurement range 296
 [19], so some mechanical restrictions apply to the placement 297
 of the OUT, transmitters, and receiving positions (Fig. 8). In 298
 order to take advantage of the whole span of the XYZ measure- 299
 ment range, scattered field samples are collected in 161 points 300
 ranging from $x = -0.6$ m to $x = 0.6$ m, placed at $Y_0 = 0$ m 301
 and $Y_0 = 1.3$ m. Five transmitting positions are interleaved 302
 among the receivers, thus resulting in $N_{tx} = 10$ transmitting 303
 positions. Transmitters and receivers are separated 5 cm 304
 in height. Horizontal polarization is considered to reduce coupling 305
 between transmitter and receiver. The imaging setup is depicted 306
 in Fig. 8: two transmitters and two receivers are connected to 307
 the ports of a vector network analyzer. The power reference 308
 level is 0 dBm for all the ports. For every receiving position 309
 along the x-axis, four S-parameters are measured, as shown in 310
 Fig. 8, corresponding to the combination of each transmitter 311
 with both receivers. 312

The positioner of the XYZ table is used to move the receivers 313
 from each side of the hallway at the same time, as shown in 314
 Fig. 8. The pair of transmitters is manually placed at five 315
 positions along the x-axis, using the XYZ positioner as reference. 316
 For every pair of transmitting positions, acquisition time takes 317
 3 min, and therefore, overall acquisition time for every OUT 318
 position is 15 min. 319

The OUT, shown in Fig. 9, is an aluminum foil-covered plastic 320
 bin with a metallic bar attached to one of the sides. Due to its 321
 translation symmetry in z-axis, it allows for 2-D analysis 322
 in an XY plane placed at $(z = h_{tx} + h_{rx}/2)$, where h_{tx} is the 323



F9:1 Fig. 9. Photograph of the OUT imaged with the proposed experimental setup.
 F9:2 Receivers are mounted on a three-axis positioner.

324 height of the transmitters, and h_{rx} the height of the receivers.
 325 As mentioned in Section II, using metal to simulate the human
 326 body skin in the Ka band is an acceptable approach due to the
 327 high conductivity of the skin in mm-wave frequency bands [16].
 328 Three positions of the OUT were considered.

329 The same data processing as in Section III has been applied.
 330 The image obtained for every position, combining the images
 331 created using all the transmitters according to (2), is depicted in
 332 Fig. 10(a). It can be noticed that, for positions 1 and 3, the front
 333 and the back of the OUT are imaged, and the sides of the OUT
 334 are visible for position 2.

335 Fig. 10(b) presents the final result combining the three OUT
 336 positions according to (3), where the OUT profile can be
 337 observed. In this case, combination is done taking the displace-
 338 ment of each individual image with respect to the center of the
 339 imaging domain. In practical, combination of the radar images
 340 for different positions of the person in the hallway can be based
 341 on video frames, linking video, and radar images.

342 In addition to the presented results, the measurement setup
 343 has been simulated, aiming to evaluate the correspondence
 344 between simulations and measurements. Results for position 2
 345 are compared in Fig. 11. Good agreement between the recon-
 346 structed parts of the OUT for simulations and measurements is
 347 obtained.

VI. 3-D CONFIGURATION

348
 349 Next, the extension from 2-D to 3-D is presented. The layout
 350 of the proposed on-the-move 3-D system is presented in Fig. 12.
 351 The setup is composed of multiple synchronized transmitters
 352 and receivers. Lateral receiving apertures of size $(X, Z) =$
 353 $(1, 2)$ m, are placed at $Y_0 = 0.75$ m. The size of the panels is
 354 chosen to provide an approximated cross-range resolution of
 355 1 cm along the z-axis and 2 cm in the x-axis.

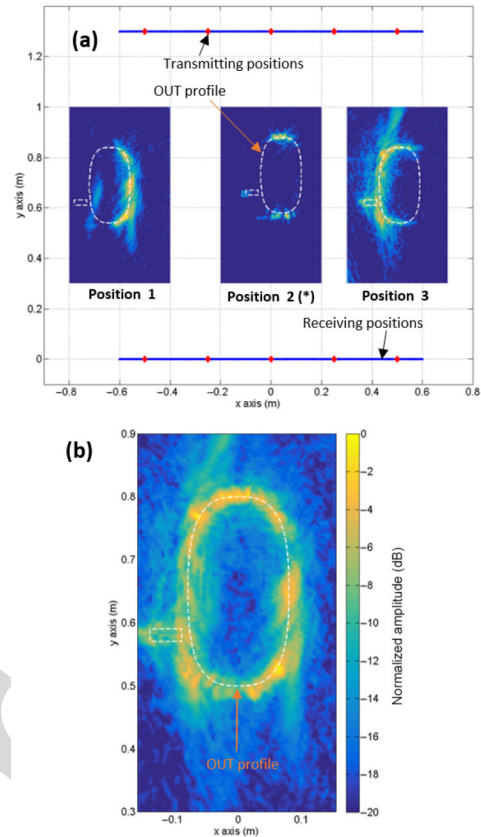


Fig. 10. Recovered OUT profile. (a) Image created on every position using
 all the transmitters according to (2). In the case of position 2, only the
 center transmitting positions ($x_{inc}^t = 0$ m) were available. (b) OUT profile when
 combining in amplitude the three images of (a).

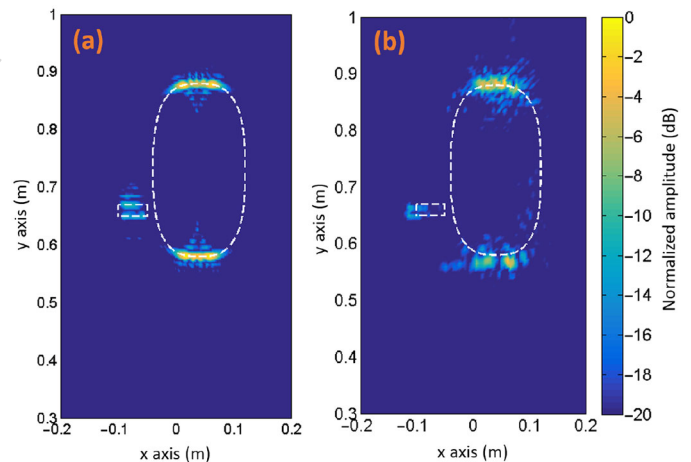
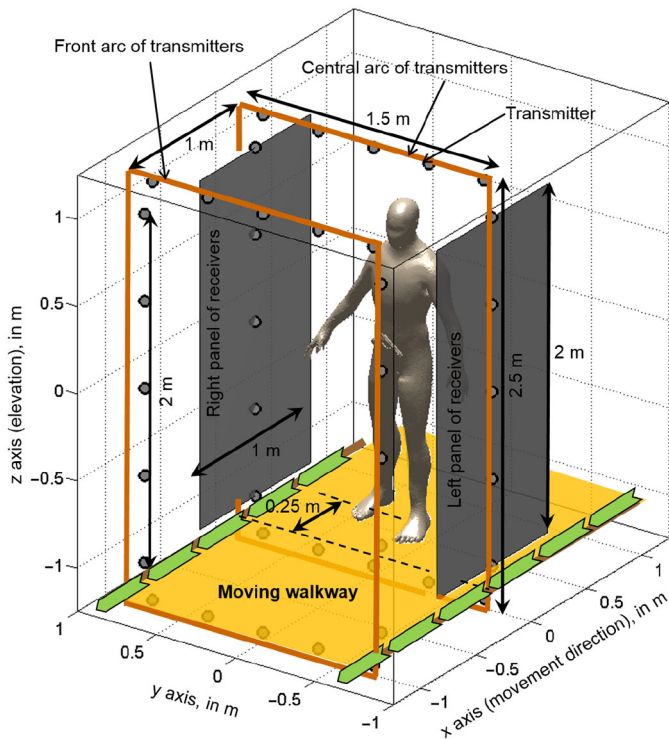


Fig. 11. Recovered OUT profile, position 2 (with center transmitting posi-
 tions). (a) From simulated data. (b) From measurements.

For this preliminary setup, Nyquist sampling requirements
 are considered for the receiving panels, thus acquiring the field
 in 201×401 receiving positions per panel. Subsampling tech-
 niques as presented in [2] and [5] combined with a modified
 FFT algorithm for multistatic imaging with subsampled arrays
 can be efficiently applied in this setup to reduce the number
 of receivers in more than 90% [2], although this analysis is
 beyond the scope of this contribution. A 15-GHz bandwidth



F12:1 Fig. 12. Layout of the mm-wave scanner for personnel screening. For the sake of
 F12:2 simplicity, just two arcs of transmitters, at $x = 0$ m, and $x = -1$ m, are
 F12:3 considered. The person under test is placed at $x = 0.25$ m.

364 (BW), from 15 to 30 GHz, is chosen, similarly to the UWB
 365 imaging system described in [5]. This BW provides an approx-
 366 imate range resolution of 1 cm, although, for near-field radar
 367 imaging, besides the frequency and aperture size, the final system
 368 lateral and range resolutions are given by (2) and (3) of
 369 [20], respectively.

370 Hallway scanner dimensions have been selected to provide
 371 a resolution similar to other mm-wave scanners, as shown in
 372 Table I. It must be reminded that the number of receiving
 373 elements can be reduced in the hallway system.

374 Concerning processing time, the fastest operational mm-
 375 wave imaging systems listed in Table I are capable to provide
 376 detection results in less than 5 s, so the scanning process can
 377 take up to 10 s taking into account that the person needs to be
 378 placed in a particular position within the scanner. For the pre-
 379 sented system, the overall scanning process would be limited
 380 by the time the person needs to go through the hallway.

381 Three arcs of transmitters, centered at $x = +1$, 0, and -1 m,
 382 and each having 20 elements evenly spaced along y - and z -axes,
 383 are considered. For the sake of simplicity, only the ones at -1
 384 and 0 m, depicted in Fig. 12, will be considered to obtain the
 385 results in this section. Some of the transmitters are placed on top
 386 and below the body to ensure the areas with larger curvature (as
 387 the top of the chest and shoulders) are reconstructed.

388 A physical optics (PO) code [21], [22] in combination with a
 389 visibility algorithm [23] has been used to predict the parts of the
 390 body model in Fig. 12 that are illuminated by every transmitter.
 391 Also, PO provides the amount of scattered field collected on the
 392 panels. Thus, it is possible to evaluate if a certain layout
 393 of transmitters is capable of illuminating the entire person after
 394 crossing the hallway and to estimate the field scattered by the

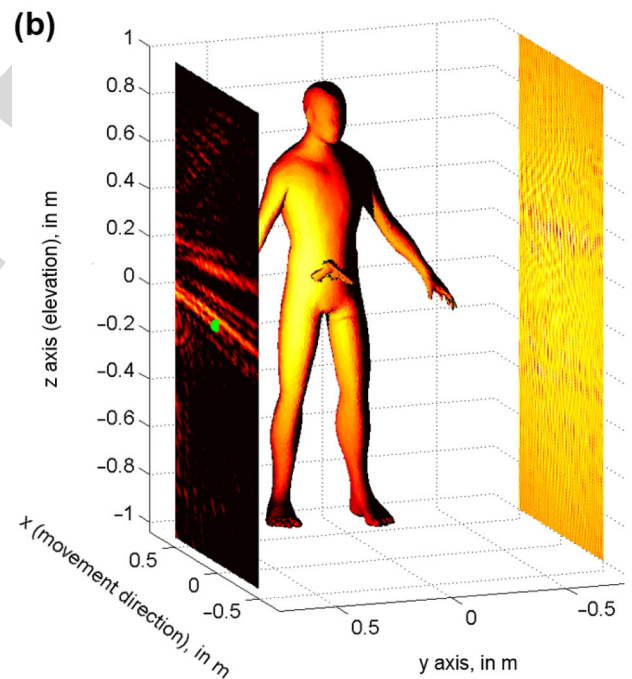
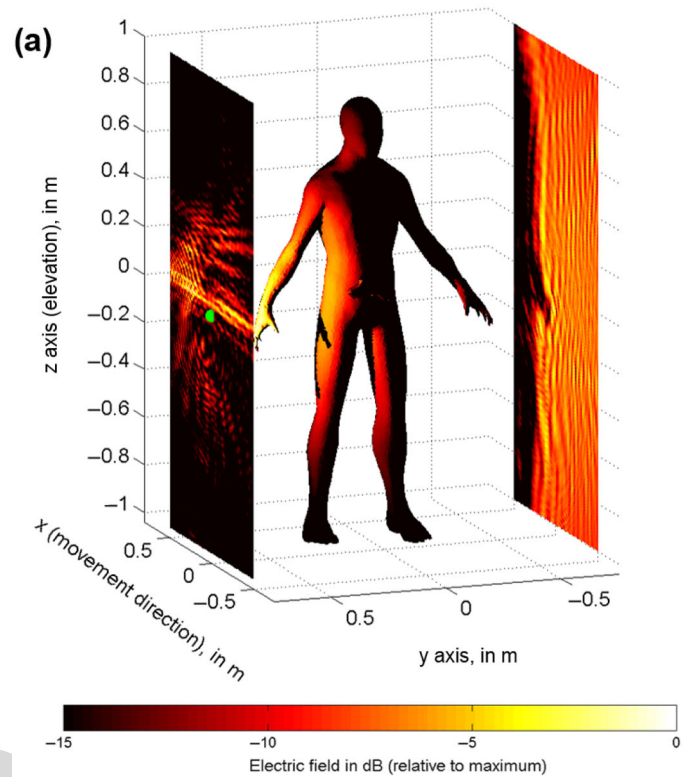
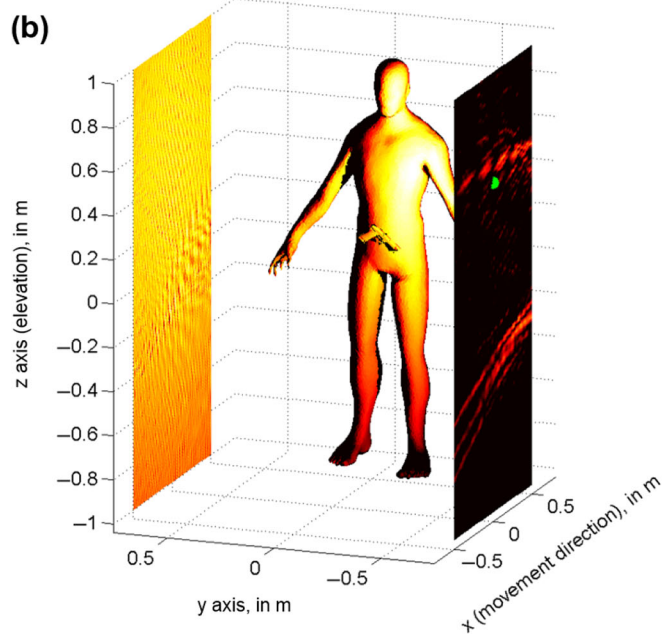
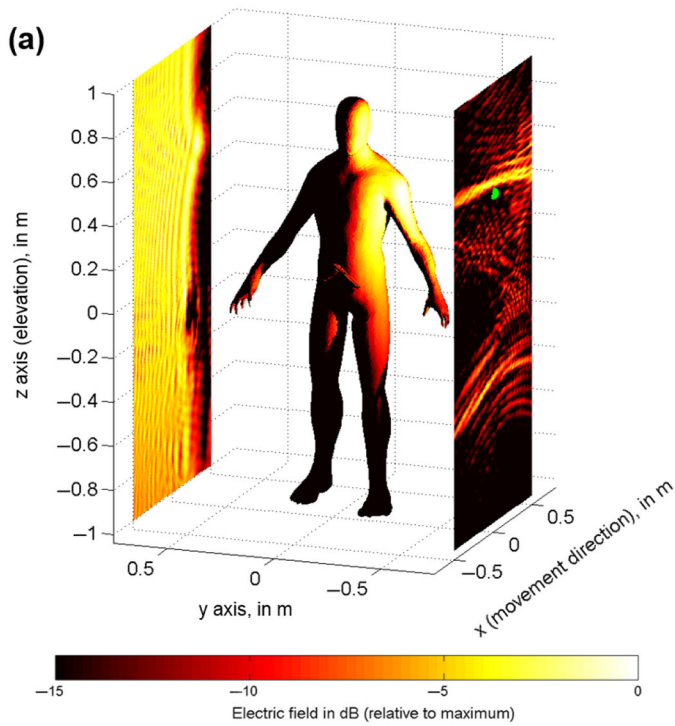


Fig. 13. Examples of human body illumination using one transmitter (high-
 F13:1 lighted in green) and scattered field on the array panels when the body model is
 F13:2 centered in (a) 0.25 m and (b) 0.75 m. F13:3

illuminated areas on the receiving panels. For these simulations, 395
 the human body is assumed to behave as a PEC in the 15–30- 396
 GHz frequency band. 397

As an example, Figs. 13 and 14 show the regions of the 398
 human body under test illuminated by two different transmitters, 399
 as well as the field received on the lateral panels. Note that, 400
 even for a single position of the person in the hallway, different 401



F14:1 Fig. 14. Examples of human body illumination using one transmitter (high-
 F14:2 lighted in green) and scattered field on the array panels when the body model is
 F14:3 centered in (a) 0.25 m and (b) 0.75 m.

402 areas of the body are illuminated. This layout increases the
 403 amount of information thanks to the spatial diversity of the
 404 multistatic illumination.

405 Regarding the inverse method to create images in this system
 406 and due to the large computational cost for the imaging,
 407 when the backpropagation is implemented in 3-D, the above-
 408 mentioned Fourier-based technique for multistatic imaging [9]
 409 has been used. The efficient use of fast Fourier transforms
 410 (FFT) provides 3-D whole body imaging in almost real time
 411 using conventional hardware.

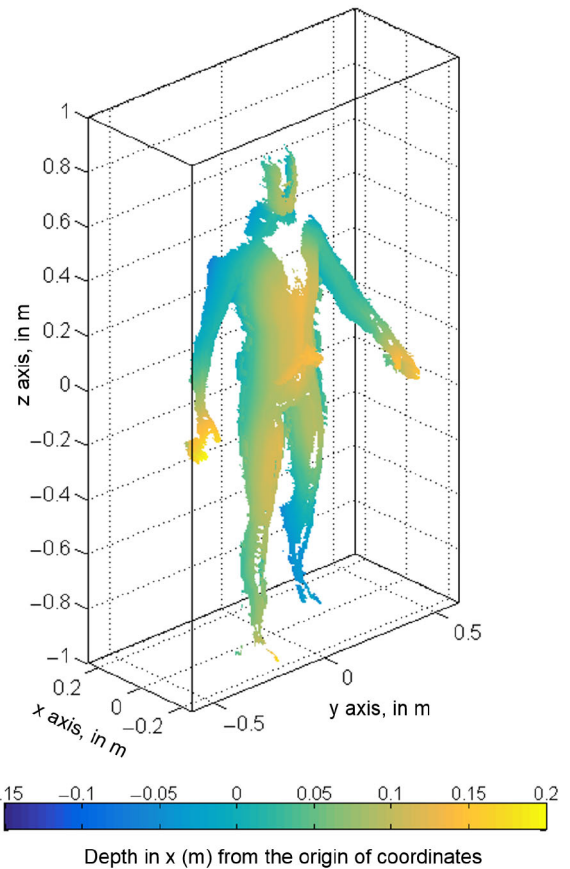
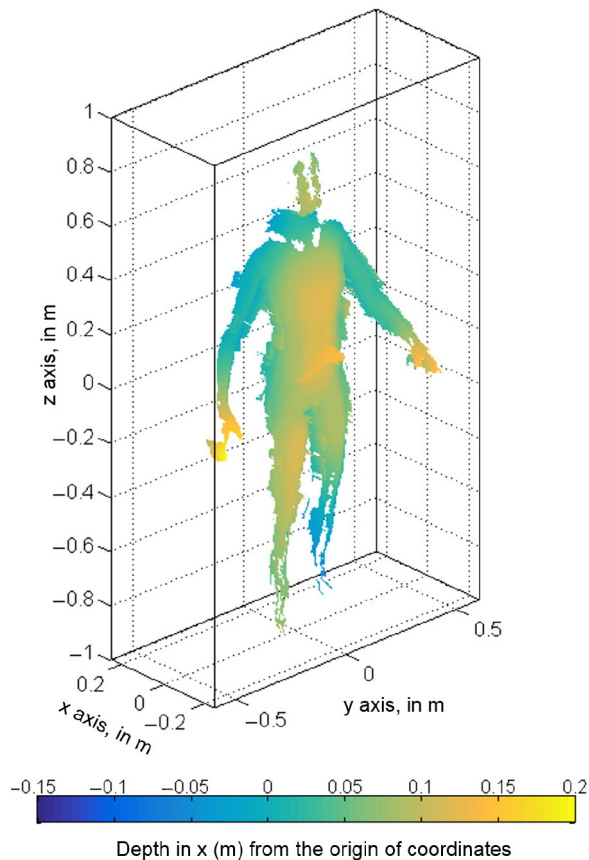


Fig. 15. Person placed at $x = 0.25$ m. Recovered human body and concealed
 object geometry from backpropagation imaging. F15:1 F15:2

412 As an application example to show the performance of the
 413 proposed configuration, an OUT consisting on a person carrying
 414 a concealed weapon in the belt has been considered. For
 415 the sake of simplicity, only two positions are analyzed: person
 416 standing at $x = 0.25$ m and at $x = 0.75$ m. In this example, the
 417 goal is to clearly illustrate the different nature of the multistatic
 418 information collected on each position, rather than a rigorous
 419 reconstruction of the whole body.

420 For every position, transmitter, and receiving panel, the
 421 amount of data to be processed is: 201×401 spatial samples \times
 422 121 frequency samples ($= 9.75 \times 10^6$ scattered field samples),
 423 which also determines the number of imaging points in the
 424 case of Fourier-based imaging [9]. A workstation with 32 cores
 425 at 2.1 GHz and 128-GB RAM was used for data processing.
 426 Overall calculation time for every transmitter was 30 s (1200 s
 427 total for the 40 used transmitters). The processing has been
 428 done using a sequential Matlab code and has not been optimized
 429 for real time imaging yet.

430 Imaging results are depicted in Figs. 15 and 16, correspond-
 431 ing to the person's placement at $x = 0.25$ m and $x = 0.75$ m,
 432 respectively. Reflectivity points above -25 dB with respect to
 433 the maximum are coded in depth according to x-axis, allowing
 434 the recovery of the human body profile and potential concealed
 435 weapons. Comparison of Figs. 15 and 16 provides a clear exam-
 436 ple of the on-the-move imaging concept effectiveness. In the
 437 case of Fig. 15 (person placed at $x = 0.25$ m), the human body
 438 sides and some areas of the chest are imaged by the system. In
 439



F16:1 Fig. 16. Person placed at $x = 0.75$ m. Recovered human body and concealed
 F16:2 object geometry from backpropagation imaging.

439 Fig. 16 (person placed at $x = 0.75$ m), the top of the chest and
 440 the shoulders are recovered.

441 In the final system, multiple images, as the two presented
 442 examples, can be created and analyzed at video rate to detect
 443 any possible threats. Algorithms for mesh generation and auto-
 444 matic thread detection, such as the one used in [8], can be
 445 applied.

VII. CONCLUSION

447 This work presented a novel concept for personnel scanning
 448 in airports and other checkpoints. Unlike the current imaging
 449 systems, the proposed system allows for continuous movement
 450 of the subject while being scanned; this will greatly increase
 451 the system throughput when compared with state-of-the-art sys-
 452 tems. This improvement is possible thanks to the use of a fully
 453 multistatic radar configuration, where some of the transmitters
 454 and receivers are separated with a subtended angle relative to
 455 the person greater than 90 degrees to capture information from
 456 all possible wave incident angles. In this way, the system is
 457 able to create a complete contour reconstruction as the person
 458 moves inside the system. The use of a small number of trans-
 459 mitters allows for fast image creation as all the transmitters can
 460 be sequentially activated in a short amount of time. 2-D and 3-D
 461 simulation-based results confirm the good imaging capabilities
 462 of the proposed system; 2-D results have also been validated
 463 using measurements. Further work will be related with the setup

optimization, including the use of sparse arrays and other tech- 464
 niques to reduce the number of receivers, and with experimental 465
 validation. 466

REFERENCES

- 467
- [1] IATA. *Checkpoint of the Future. Executive Summary* [Online]. Available: 468
<http://www.iata.org/whatwedo/security/Documents/cof-executive-> 469
 summary.pdf, accessed on Mar. 16, 2015. 470Q2
 - [2] S. S. Ahmed, A. Schiessl, F. Gumbmann, M. Tiebout, S. Methfessel, 471
 and L. Schmidt, "Advanced microwave imaging," *IEEE Microw. Mag.*, 472
 vol. 13, no. 6, pp. 26–43, Sep./Oct. 2012. 473
 - [3] S. S. Ahmed, "Personnel screening with advanced multistatic imaging 474
 technology," in *Proc. SPIE Defense Secur. Sens.*, 2013, p. 87150B. 475
 - [4] D. Sheen, D. McMakin, and T. Hall, "Three-dimensional millimeter-wave 476
 imaging for concealed weapon detection," *IEEE Trans. Microw. Theory* 477
Techn., vol. 49, no. 9, pp. 1581–1592, Sep. 2001. 478
 - [5] X. Zhuge and A. Yarovoy, "A sparse aperture MIMO-SAR-based UWB 479
 imaging system for concealed weapon detection," *IEEE Trans. Geosci.* 480
Remote Sens., vol. 49, no. 1, pp. 509–518, Jan. 2011. 481
 - [6] D. M. Sheen, D. L. McMakin, and T. E. Hall, "Combined illumination 482
 cylindrical millimeter-wave imaging technique for concealed weapon 483
 detection," in *Proc. AeroSense*, 2000, pp. 52–60. 484
 - [7] Y. Rodríguez-Vaqueiro, Y. Álvarez López, B. Gonzalez-Valdes, 485
 J. A. Martínez, F. Las-Heras, and C. M. Rappaport, "On the use of 486
 compressed sensing techniques for improving multistatic millimeter- 487
 wave portal-based personnel screening," *IEEE Trans. Antennas Propag.*, 488
 vol. 62, no. 1, pp. 494–499, Jan. 2014. 489
 - [8] B. Gonzalez-Valdes, Y. Alvarez-Lopez, J. A. Martinez-Lorenzo, F. Las 490
 Heras Andres, and C. M. Rappaport, "On the use of improved imag- 491
 ing techniques for the development of a multistatic three-dimensional 492
 millimeter-wave portal for personnel screening," *Prog. Electromagn.* 493
Res., vol. 138, pp. 83–98, 2013. 494
 - [9] Y. Alvarez *et al.*, "Fourier-based imaging for multistatic radar systems," 495
IEEE Trans. Microw. Theory Techn., vol. 62, no. 8, pp. 1798–1810, Aug. 496
 2014. 497
 - [10] G. Yates, A. Horne, A. Blake, and R. Middleton, "Bistatic SAR image 498
 formation," *Inst. Elect. Eng. Proc. Radar Sonar Navigat.*, vol. 153, no. 3, 499
 pp. 208–213, Jun. 2006. 500
 - [11] R. Burkholder, I. Gupta, and J. Johnson, "Comparison of monostatic and 501
 bistatic radar images," *IEEE Trans. Antennas Propag. Mag.*, vol. 45, no. 3, 502
 pp. 41–50, Jun. 2003. 503
 - [12] B. Gonzalez-Valdes, C. Rappaport, and J. A. Lorenzo-Martinez, "On- 504
 the-move active millimeter wave interrogation system using a hallway 505
 of multiple transmitters and receivers," in *Proc. IEEE Antennas Propag.* 506
Soc. Int. Symp. (APSURSI), 2014, pp. 1107–1108. 507
 - [13] B. Gonzalez-Valdes, C. Rappaport, and J. Martinez-Lorenzo, "On the 508
 move millimeter wave interrogation system with a hallway of multiple 509
 transmitters and receivers," U.S. Patent 14 562 094, Dec. 5, 2014. 510
 - [14] M. Soumekh, "Bistatic synthetic aperture radar inversion with application 511
 in dynamic object imaging," *IEEE Trans. Signal Process.*, vol. 39, no. 9, 512
 pp. 2044–2055, Sep. 1991. 513
 - [15] Y. Alvarez, J. Martinez, F. Las-Heras, and C. Rappaport, "An inverse 514
 fast multipole method for imaging applications," *IEEE Antennas Wireless* 515
Propag. Lett., vol. 10, pp. 1259–1262, Nov. 2011. 516
 - [16] D. Andreuccetti, R. Fossi, and C. Petrucci, "An Internet resource for the 517
 calculation of the dielectric properties of body tissues in the frequency 518
 range 10 Hz–100 GHz," Internet document, 1997 [Online]. Available: 519
<http://niremf.ifac.cnr.it/tissprop/>, accessed on Sep. 15, 2015, IFAC-CNR, 520
 Florence, Italy, 1997, based on data published by C. Gabriel *et al.* in 1996. 521
 - [17] A. W. Morgenthaler and C. M. Rappaport, "Scattering from lossy dielectric 522
 objects buried beneath randomly rough ground: Validating the semi- 523
 analytic mode matching algorithm with 2-D FDFD," *IEEE Trans. Geosci.* 524
Remote Sens., vol. 39, no. 11, pp. 2421–2428, Nov. 2001. 525
 - [18] C. M. Rappaport, Q. Dong, E. Bishop, A. Morgenthaler, and 526
 M. E. Kilmer, "Finite difference frequency domain (FDFD) modeling of 527
 two dimensional TE wave propagation," in *Proc. URSI Symp. Conf.*, Pisa, 528
 Italy, 2004. 529Q3
 - [19] A. Arbolea, Y. Alvarez, and F. Las-Heras, "Millimeter and submillimeter 530
 planar measurement setup," in *Proc. IEEE Antennas Propag. Soc. Int.* 531
Symp. (APSURSI), 2013, pp. 1–2. 532
 - [20] S. S. Ahmed, A. Schiessl, and L.-P. Schmidt, "A novel active real-time 533
 digital-beamforming imager for personnel screening," in *Proc. 9th Eur.* 534
Conf. Synth. Aperture Radar (EUSAR), Apr. 2012, pp. 178–181. 535

- 536 [21] J. Meana, J. Martinez-Lorenzo, F. Las-Heras, and C. Rappaport, "Wave
537 scattering by dielectric and lossy materials using the modified equivalent
538 current approximation (MECA)," *IEEE Trans. Antennas Propag.*, vol. 58,
539 no. 11, pp. 3757–3761, Nov. 2010.
- 540 [22] L. E. Tirado, J. A. Martinez-Lorenzo, B. Gonzalez-Valdes, C. Rappaport,
541 O. Rubinos-Lopez, and H. Gomez-Sousa, "GPU implementation of
542 the modified equivalent current approximation (MECA) method," *Appl.*
543 *Comput. Electromagn. Soc. J.*, no. 9, Sep. 2012.
- 544 [23] J. Gutiérrez Meana, F. L. Las Heras Andrés, and J. Á. Martínez Lorenzo,
545 "A comparison among fast visibility algorithms applied to computational
546 electromagnetics," *Appl. Comput. Electromagn. Soc. J.*, 2009.



Borja Gonzalez-Valdes (M'xx) received the B.S. and Ph.D. degrees in electrical engineering from the University of Vigo, Vigo, Spain, in 2006 and 2010, respectively.

From 2006 to 2010, he was with the Antenna and Optical Communications Group, University of Vigo. From 2008 to 2009, he was a Visiting Researcher with the Gordon Center for Subsurface Sensing & Imaging Systems, Northeastern University, Boston, MA, USA. In 2011, he joined the Awareness and

547
548
549
550
551
552
553
554
555
556
557
558
559
560
561
Localization of Explosives-Related Threats Center of Excellence, Northeastern University. Since 2015, he has been a Postdoctoral Researcher affiliated with the AtlantTIC Research Center, University of Vigo. His research interests include antenna design, inverse scattering, radar, advanced imaging techniques, and THz technology.



Yuri Álvarez (S'06–M'09–SM'15) was born in Langreo, Spain, in 1983. He received the M.S. and Ph.D. degrees in telecommunication engineering from the University of Oviedo, Gijn, Spain, in 2006 and 2009, respectively.

He was a Visiting Scholar at the Department of Electrical Engineering and Computer Science, Syracuse University, Syracuse, NY, USA, in 2006 and 2008; a Visiting Postdoc at the Gordon Center for Subsurface Sensing and Imaging Systems (CenSSIS)ALERT (Awareness and Localization of

562
563
564
565
566
567
568
569
570
571
572
573
574
575
576
577
578
579
Explosive Related Threats) Center of Excellence, Northeastern University, Boston, MA, USA, from 2011 to 2014; and a Visiting Postdoc at ELEDIA Research Center, Trento, Italy, in 2015. He is currently an Assistant Professor with the Signal Theory and Communications, University of Oviedo, Gijn, Spain. His research interests include antenna diagnostics, antenna measurement techniques, RF techniques for indoor location, inverse scattering and imaging techniques, and phaseless methods for antenna diagnostics and imaging.

580 Dr. Alvarez was the recipient of the 2011 Regional and National Awards to
581 the Best Ph.D. Thesis on Telecommunication Engineering (category: security
582 and defense).



Yolanda Rodriguez-Vaqueiro (S'xx) received the B.S. and M.S. degrees in electrical engineering from the University of Vigo, Vigo, Spain, in 2009, and the Ph.D. degree in electrical engineering from Northeastern University, Boston, MA, USA, in 2015 (after defending her thesis: Compressive Sensing for Electromagnetic Imaging Using a Nesterov-Based Algorithm).

583
584
585
586
587
588
589
590
591
592
593
594
595
596
597
598
599
600
601
602
603
604
605
606
She is a Postdoctoral Researcher affiliated with the AtlantTIC Research Center, University of Vigo. In 2011, she obtained a Research Assistant grant from the ALERT (Awareness and Localization of Explosive Related Threats) Center of Excellence, Northeastern University. She was also granted as a Junior Researcher with the University of Vigo.

Dr. Rodriguez-Vaqueiro was the recipient of the Research-Impact Award by the Department of Electrical and Computer Engineering, Northeastern University (for her work during the Ph.D. studies), the Best Paper Award in the 2012 IEEE Homeland Security Conference, Honorable Mention in the Student Paper Competition in the 2013 IEEE APS/URSI Conference, the Best Paper Award in the 2014 European Conference on Antennas and Propagation, the Burke/Yannas Award to the most original research study in the field of bioengineering in the 2015 American Burn Association (ABA) Meeting, and the Research-Impact Award by the Department of Electrical and Computer Engineering, Northeastern University, in May 2015.



607
608
609
610
611
612
613
614
615
616
617
618
619
research interests include antenna diagnostics and measurement systems and techniques and high-frequency imaging techniques and applications.



Antonio García-Pino (S'87–M'89–SM'05) was born in Valdemoro, Madrid, Spain, in 1962. He received the M.S. and Ph.D. degrees in telecommunications engineering from the Polytechnic University of Madrid (UPM), Madrid, Spain, in 1985 and 1989, respectively.

620
621
622
623
624
625
626
627
628
629
630
631
632
633
634
635
636
637
638
639
640
641
642
643
644
645
646
647
648
649
650
651
652
653
654
655
656
657
658
659
660
661
662
663
664
665
666
667
668
669
670
671
672
673
674
675
From 1985 to 1989, he was a Research Assistant with the Radiation Group, UPM. He joined as an Associate Professor with the Department of Technologies of Communications, University of Vigo, Vigo, Spain, in 1989, becoming Full Professor

in 1994. In 1993, he was a Visiting Researcher at the Center for Electromagnetics Research, Northeastern University, Boston, MA, USA. From 2006 to 2010, he was the Vice-Rector of Academic Organization and Faculty, and currently, he is the Director of the International Doctoral School, both at University of Vigo. His research interests include shaped-reflector antennas for communication and radar applications, high-frequency backscattering, computational electromagnetics, and THz technology. In these topics, he has authored more than 100 technical papers in journal and conferences and he has been an advisor of 14 Ph.D. thesis.



Carey M. Rappaport (SM'96–F'06) received the S.B. degree in mathematics, the S.B., S.M., and E.E. degrees in electrical engineering in 1982, and the Ph.D. degree in electrical engineering in 1987 from the Massachusetts Institute of Technology (MIT), Cambridge, MA, USA.

646
647
648
649
650
651
652
653
654
655
656
657
658
659
660
661
662
663
664
665
666
667
668
669
670
671
672
673
674
675
He was a Teaching and Research Assistant with MIT from 1981 until 1987, and during the summers at COMSAT Labs, Clarksburg, MD, USA, and the Aerospace Corp., El Segundo, CA, USA. He joined the faculty at Northeastern University,

Boston, MA, USA, in 1987. He has been a Professor of Electrical and Computer Engineering since July 2000. In 2011, he was appointed as a College of Engineering Distinguished Professor. In fall 1995, he was a Visiting Professor of Electrical Engineering at the Electromagnetics Institute, Technical University of Denmark, Lyngby, Denmark, as part of the W. Fulbright International Scholar Program. In the second half of 2005, he was a Visiting Research Scientist at the Commonwealth Scientific Industrial and Research Organisation (CSIRO), Epping, Australia. He has consulted for CACI, Alion Science and Technology, Inc., Geo-Centers, Inc., PPG, Inc., and several municipalities on wave propagation and modeling, and microwave heating and safety. He was the Principal Investigator of an ARO-sponsored Multidisciplinary University Research Initiative on Humanitarian Demining, the Co-Principal Investigator of the NSF-sponsored Engineering Research Center for Subsurface Sensing and Imaging Systems (CenSSIS), and the Co-Principal Investigator and Deputy Director of the DHS-sponsored Awareness and Localization of Explosive Related Threats (ALERT) Center of Excellence. He has authored more than 400 technical journal and conference papers in the areas of microwave antenna design, electromagnetic wave propagation and scattering computation, and bioelectromagnetics, and has received two reflector antenna patents, two biomedical device patents, and four subsurface sensing device patents.

Prof. Rappaport is a member of Sigma Xi and Eta Kappa Nu professional honorary societies. He was the recipient of the IEEE Antenna and Propagation Society's H. A. Wheeler Award for the Best Applications Paper, as a Student in 1986.

676
677
678
679
680
681
682
683
684
685
686
687
688
689
690
691
692
693
694
695
696
697
698
699
700
701
702
703



Fernando Las-Heras (M'86–SM'08) received the M.S. and Ph.D. degrees in telecommunication engineering from the Technical University of Madrid (UPM), Madrid, Spain, in 1987 and 1990, respectively.

He was a National Graduate Research Fellow (1988–1990), and he held a position of Associate Professor with the Department of Signal, Systems, and Radiocommunications, UPM (1991–2000). From December 2003, he holds a Full Professor position with the University of Oviedo, Oviedo, Spain, where

he was the Vice-Dean for Telecommunication Engineering, Technical School of Engineering, Gijón, Spain (2004–2008). As of 2001, he was the Head of the Research Group Signal Theory and Communications TSC-UNIOVI, Department of Electrical Engineering, University of Oviedo. He was a Visiting Lecturer at the National University of Engineering, Rímac Lima, Peru, in 1996, a Visiting Researcher at Syracuse University, Syracuse, NY, USA, in 2000, and a short-term Visiting Lecturer at ESIGELEC, France, from 2005 to 2011. He held the Telefónica Chair on RF Technologies, ICTs applied to Environment and ICTs and Smartcities with the University of Oviedo (2005–2015). He has authored more than 300 articles published in academic journals and proceedings of international conferences, mainly in the areas of antenna design and the inverse electromagnetic problem with applications in diagnostic, measurement and synthesis of antennas, phaseless techniques, propagation, and microwave to THz imaging and localization, as well as in engineering education.

Dr. Las-Heras was a Member of the Board of Directors of the IEEE Spain Section (2012–2015), and from 2010, he was a Member of the Science, Technology, and Innovation Council of Asturias, Asturias, Spain.



Jose A. Martinez-Lorenzo (M'xx) received the B.S./M.S. degree in 2002 and the Ph.D. degree in 2005 from the University of Vigo, Vigo, Spain, both in electrical engineering.

He joined the faculty at University of Oviedo, Gijon, Spain, in 2004, where he was an Assistant Professor with the Department of Signal Theory and Communications. In 2006, he joined Bernard M. Gordon Center for Subsurface Sensing and Imaging Systems, Northeastern University, Boston, MA, USA. In 2010, he was a Research Assistant

Professor with the Department of ECE, Northeastern University. Since August 2013, he has been held a joint appointment with the Departments of MIE and ECE as a Tenure-Track Assistant Professor. He is an Active Member of Awareness and Localization of Explosives-Related Threats (ALERT) a DHS Center of Excellence awarded to Northeastern University. He has authored more than 140 technical journal and conference papers. His research interests include the understanding, modeling, and solving complex engineering problems, with an emphasis on mechanical and electromagnetic sensing and imaging methods for security and biomedical applications (i.e., explosive detection, breast cancer detection).

Prof. Martinez-Lorenzo has received funding from multiple agencies, including: DHS, DARPA, NSF, US Army, and the European Space Agency (ESA). He led the team that won the Best Paper Award in the 2012 IEEE Conference on Technologies for Homeland Security, for the paper on a compressed sensing approach for detection of explosive threats at standoff distances using a passive array of scatterers.

704
705
706
707
708
709
710
711
712
713
714
715
716
717
718
719
720
721
722
723
724
725
726
727
728
729
730

QUERIES

- Q1: Please provide captions for Fig. 3 subparts.
- Q2: Please provide year of publication for Ref. [1].
- Q3: Please provide page range for Refs. [18], [22], and [23].
- Q4: Please provide volume number for Ref. [22] and [23].
- Q5: Please provide the membership history (year) of the authors Borja Gonzalez-Valdes, Yolanda Rodriguez-Vaqueiro, and Jose A. Martinez-Lorenzo.
- Q6: Please provide year of completion for the S.B. degree in Mathematics, S.B., S.M. degrees in electrical engineering of author "Carey M. Rappaport."

IEEE PROOF

Millimeter Wave Imaging Architecture for On-The-Move Whole Body Imaging

Borja Gonzalez-Valdes, *Member, IEEE*, Yuri Álvarez, *Senior Member, IEEE*,
Yolanda Rodriguez-Vaqueiro, *Student Member, IEEE*, Ana Arboleya-Arboleya,
Antonio García-Pino, *Senior Member, IEEE*, Carey M. Rappaport, *Fellow, IEEE*,
Fernando Las-Heras, *Senior Member, IEEE*, and Jose A. Martinez-Lorenzo, *Member, IEEE*

Abstract—This paper presents a novel interrogation system that combines multiple millimeter wave transmitters and receivers to create real-time high-resolution radar images for personnel security screening. The main novelty of the presented system is that the images can be created as the person being screened continuously moves across a corridor where the transmitters and receivers, working in a fully coherent architecture, are distributed. As the person moves, the transmitters and receivers are sequentially activated to collect data from different angles to inspect the whole body. Multiple images, similar to video frames, are created and examined to look for possible anomalies such as concealed threats. Two-dimensional (2-D) and three-dimensional (3-D) setups have been simulated to show the feasibility of the proposed system. The simulation results in 2-D have been validated using measurements.

Index Terms—Backpropagation imaging, checkpoint, fast Fourier transform (FFT), imaging systems, multistatic radar system.

I. INTRODUCTION

IN homeland security applications, there is an increasing demand for methods to improve personnel screening for concealed object and contraband detection at security checkpoints. In this context, active nearfield millimeter-wave (mm-wave) imaging radar systems are able to provide high-resolution imaging at an affordable cost. The object of interest is first illuminated by mm waves and then the scattered field is

Manuscript received June 18, 2015; revised January 11, 2016; accepted February 18, 2016. Date of publication XXXX XX, XXXX; date of current version XXXX XX, XXXX. This work was supported in part by the Ministerio de Ciencia e Innovación of Spain/FEDER under project MIRIEM-TEC2014-54005-P, in part by the Gobierno del Principado de Asturias through the PCTI 2013-2017, GRUPIN14-114, in part by the Spanish Government under project TACTICA, in part by the European Regional Development Fund (ERDF), in part by the Galician Regional Government under Projects CN2012/279, CN2012/260 (AtlantTIC) and the Plan I2C (2011–2015), and in part by the Science and Technology Directorate, U.S. Department of Homeland Security under the Award Number 2008-ST-061-ED0001.

B. Gonzalez-Valdes, Y. Rodriguez-Vaqueiro, and A. García-Pino are with the Atlantic Research Center, Universidad de Vigo, 36310 Vigo, Spain (e-mail: bgvaldes@com.uvigo.es; yrvaqueiro@com.uvigo.es; agpino@com.uvigo.es).

Y. Álvarez, A. Arboleya Arboleya, and F. Las-Heras are with the Area of Signal Theory and Communications, Department of Electrical Engineering, Universidad de Oviedo, E-33203 Gijón, Spain (e-mail: yalopez@tsc.uniovi.es; aarboleya@tsc.uniovi.es; flasheras@tsc.uniovi.es).

C. M. Rappaport and J. A. Martinez are with the ALERT Center, Northeastern University, Boston, MA 02115 USA (e-mail: rappaport@ece.neu.edu; jmartine@ece.neu.edu).

Color versions of one or more of the figures in this paper are available online at <http://ieeexplore.ieee.org>.

Digital Object Identifier 10.1109/TAP.2016.2539372

measured and processed to reconstruct the surface (or volume) of the object.

The development of checkpoints that allow high passenger flow is becoming a priority. This has motivated the design of mm-wave imaging systems that minimize passenger inconvenience.

The International Air Transport Association (IATA) has defined several specifications that future checkpoints for personnel screening should meet. Novel paradigms in the design of the checkpoints specify that “from 2020 and beyond it is envisaged that the passenger will be able to flow through the security checkpoint without interruption unless the advanced technology identifies a potential threat,” [1] (page 14).

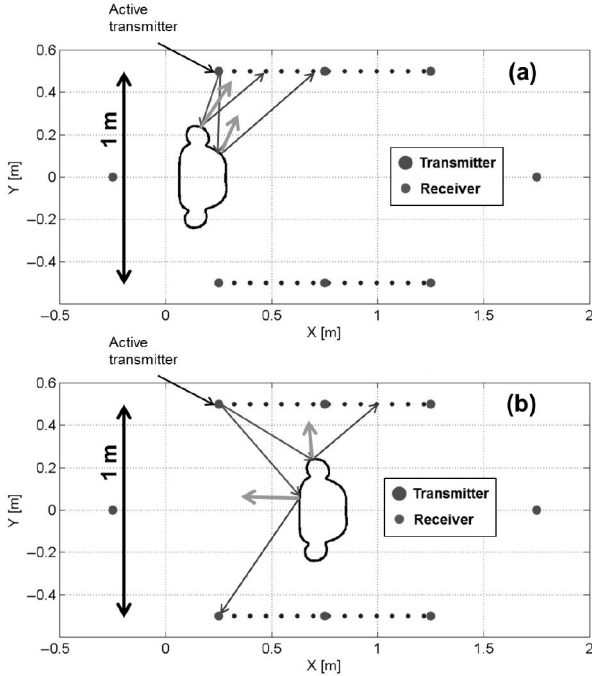
In [1], a computer graphics design of the checkpoint of the future proposed by IATA is presented. The novelty with respect to existing architectures is the inclusion of a beltway or hallway to avoid passenger flow interruption.

Current state-of-the-art mm-wave imaging systems for security screening require people to enter and stand in front of the scanning system. Mm-wave generation and acquisition can be achieved using static arrays of transmitters and receivers [2], [3], or using movable arrays to create planar [4], [5], or cylindrical [6]–[8] acquisition domains. Most of them are based on monostatic radar and Fourier inversion [2]–[6]. Monostatic imaging systems are cost effective, but they are only able to reconstruct surfaces that create specular reflection and they are not well suited for imaging scattering objects with sudden profile variations [9]. Further, they are prone to dihedral artifacts as described in [8], [10], and [11].

Based on the new checkpoint architecture proposed by the IATA, this paper introduces a novel concept for mm-wave scanning system for personnel screening. The proposed imaging system does not include any mechanical movement, and whole body imaging is obtained taking advantage of the movement of the person under test when passing through the system on a moving walkway.

The main contribution of this paper is the introduction of this novel architecture, called on-the-move imaging [12], [13], that, to the best of the author’s knowledge, has not been previously conceived nor demonstrated.

This paper is structured as follows. Section II describes the proposed mm-wave screening system. Imaging algorithm for multistatic setups is briefly described in Section III. Proof-of-concept is validated through two-dimensional (2-D) simulation



F1:1 Fig. 1. On-the-move imaging concept. OUT movement between the two walls
 F1:2 of radar antennas provides multiple points-of-view for every transmitter and
 F1:3 receiver, thus increasing multistatic information. (a) and (b) represent two
 F1:4 different OUT positions within the hallway.

76 examples in Section IV, and measurement results in Section V.
 77 Extension to two-dimensional (3-D) whole human body imag-
 78 ing is described and validated in Section VI. Finally, the
 79 conclusion is presented in Section VII.

80 II. ON-THE-MOVE HALLWAY CONCEPT

81 The novel mm-wave on-the-move imaging system for per-
 82 sonnel screening takes advantage of: 1) the movement of the
 83 person when passing through the imaging system and 2) a mul-
 84 tistatic radar configuration, where some of the transmitters and
 85 receivers are separated with a subtended angle relative to the
 86 person equal or greater than 90° to capture information from
 87 all possible wave incident and scattering angles.

88 A top view of the suggested multistatic architecture is plot-
 89 ted in Fig. 1. Several transmitters (red dots) and receivers (blue
 90 dots) are placed on the sides of the hallway. The person moves
 91 along the security checkpoint on a moving walkway.

92 The imaging radar system takes advantage of multiple inci-
 93 dence angles that illuminate different areas of the person
 94 depending on the active transmitter and the placement of the
 95 person within the hallway, as illustrated in Fig. 1. A single
 96 transmitter can illuminate different areas of the person while
 97 crossing the hallway. Reciprocally, the scattered field is col-
 98 lected by different receivers depending on the transmitting
 99 element and the current position of the person. This is illus-
 100 trated with the red and blue arrows in Fig. 1 that represent
 101 direct reflection contributions given by the incident angle and
 102 the normal to the surface according to Snell's law.

103 Multistatic information can be incremented by placing trans-
 104 mitters at the hallway ends. For practical implementation, this

TABLE I
 COMPARISON WITH STATE-OF-THE-ART MM-WAVE IMAGING SYSTEMS

Reference	Scanning area (cm) ¹	PSF (mm) ²	Frequency band (GHz)	Number of antennas
On-the-move	100×200^3	10×10	15 – 30	2×80601 Rx 60 Tx
UWB MIMO array, [5]	50×130	10×10	2.8 – 19.5	4 Tx 8 Rx, Height motion.
Flat 2-D array, [2]	100×200	3.0×1.5	72 – 80	3072 Tx 3072 Rx
Linear array, vertical movement [4]	72.6 Movable 2 m in height	10.0×3.8	27 – 33	66 Tx, 66 Rx, Height motion

¹Scanning area size: width \times height.

²PSF (point spread function): range \times cross range.

³Receiving panels size.

would partially block the persons path. This is solved in the 3-D 105
 case placing the receivers at the hallway ends below and above 106
 the moving walkway. 107

For every transmitter, the scattered field is collected on the 108
 receiving arrays placed on the hallway sides, and for every 109
 receiving array, a reflectivity image is recovered. The reflectiv- 110
 ity images associated with each transmitter are coherently com- 111
 bined. This configuration assumes that, for a single position, 112
 the body remains still while all the transmitters are sequen- 113
 tially activated and the scattered field is collected by the receivers. 114
 In this sense, and since the acquisition on the receivers can be 115
 done in parallel, the use of a low number of transmitters is desir- 116
 able. A fully electronic scanning system similar to the one in [3] 117
 would easily allow for such an acquisition procedure. 118

A critical aspect in the design of the imaging system is the 119
 selection of the frequency band. Table I shows a comparison 120
 among the proposed hallway concept and some of the exist- 121
 ing mm-wave scanning systems. It can be observed that, for 122
 a given size of the scanner, higher frequency bands provide 123
 better cross-range resolution, at the expense of losing dynamic 124
 range due to free-space propagation losses. Furthermore, cloth- 125
 ing becomes less transparent for these higher frequency bands, 126
 and radiofrequency hardware becomes more expensive. The 127
 work presented in [5] addresses the aforementioned drawbacks 128
 introducing an ultra-wideband (UWB) imaging system. In addi- 129
 tion to the improved range resolution and dynamic range, the 130
 novelty of this study is the fact that the sampling rate can be 131
 relaxed by taking advantage of grating lobes cancellation in 132
 UWB arrays, which will be of interest concerning practical 133
 implementation of the on-the-move architecture. 134

135 III. IMAGING ALGORITHM

136 Practical mm-wave scanning system implementation 136
 demands real-time imaging capabilities. Standard backprop- 137
 agation techniques [14] require millions of calculations for 138
 electrically large acquisition and imaging domains. To illus- 139
 trate the numerical magnitude of the problem, typical values 140
 for acquisition points and imaging voxels are 10^5 and 10^7 , 141

142 respectively, assuming an operational frequency of 30 GHz
 143 ($\lambda = 1$ cm) and sampling every half wavelength in both
 144 domains according to Nyquist criterion.

145 The reflectivity function on a volumetric domain
 146 $\rho_t(x', y', z')$ can be recovered from the scattered field
 147 $E_{scatt}^t(f, x, z)$ acquired on a flat receiving aperture placed at
 148 $y = Y_0$, by solving the following integral equation [9], [14],
 149 when the t th (with t from 1 to N_{tx}) of a group of transmitters
 150 is active

$$\begin{aligned} \rho_t(x', y', z') &= \iiint E_{scatt}^t(f, x, z) e^{+jk((x-x')^2 + (Y_0 - y')^2 + (z-z')^2)^{1/2}} \\ & e^{+jk((x_{inc}^t - x')^2 + (y_{inc}^t - y')^2 + (z_{inc}^t - z')^2)^{1/2}} df dx dz \end{aligned} \quad (1)$$

151 where $(x_{inc}^t, y_{inc}^t, z_{inc}^t)$ denotes the position of the t th point
 152 source-like transmitter, $k = 2\pi f/c$, y -axis is the range axis
 153 (depth), x - and z -axes are horizontal and vertical cross ranges,
 154 and f is the frequency.

155 Fast propagation techniques, such as the inverse fast multi-
 156 pole method, have been proposed [15], reducing the calculation
 157 time by several orders of magnitude. Moreover, (1) can be par-
 158 allelized taking advantage of GPU hardware. However, these
 159 solutions are still too computationally expensive for applica-
 160 tions requiring real-time imaging.

161 Fourier-based techniques have been widely used in mono-
 162 static setups for real-time imaging [3]–[5], thanks to the fact
 163 that plane wave incidence can be considered during the inver-
 164 sion. Multistatic setups require different Fourier processing as
 165 the transmitter and receiver are placed in different positions. A
 166 novel Fourier-based imaging technique, totally suitable for the
 167 proposed hallway-based on-the-move imaging system, is pre-
 168 sented in [9]. The idea is to decompose the imaging domain in
 169 smaller regions where an incident spherical wave can be locally
 170 treated as a plane wave. Imaging calculations for every region
 171 can be carried out in parallel, without jeopardizing the required
 172 real-time capabilities of the multistatic imaging system.

173 When multiple transmitters are used, the final reconstruc-
 174 tion for a certain voxel placed in (x', y', z') can be obtained
 175 by combining the images generated by each transmitter as

$$\rho(x', y', z') = \sum_{t=1}^{N_{tx}} \rho_t(x', y', z'). \quad (2)$$

176 This formulation assumes all the transmitters and receivers
 177 work in a fully coherent configuration using a clock signal that
 178 provides common phase reference.

179 IV. 2-D RESULTS

180 The proposed on-the-move imaging is first validated using a
 181 2-D example. The frequency band ranges from 15 to 30 GHz,
 182 sampled every 300-MHz frequency steps and providing 1-cm
 183 range resolution. Two 1-m width lateral arrays of receivers
 184 with 50 evenly spaced elements are placed at $Y_0 = -0.6$ m
 185 and $Y_0 = 0.6$ m. Five transmitters are interleaved among each

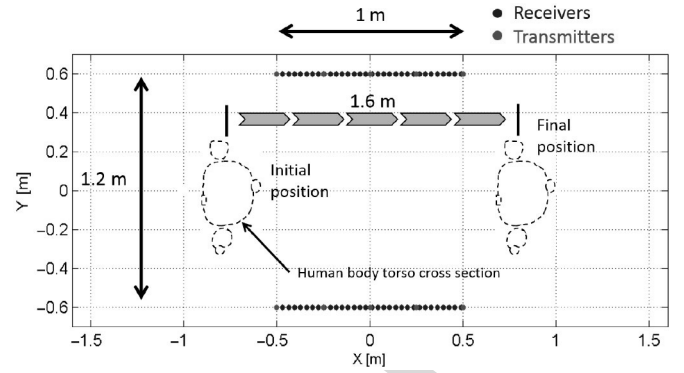


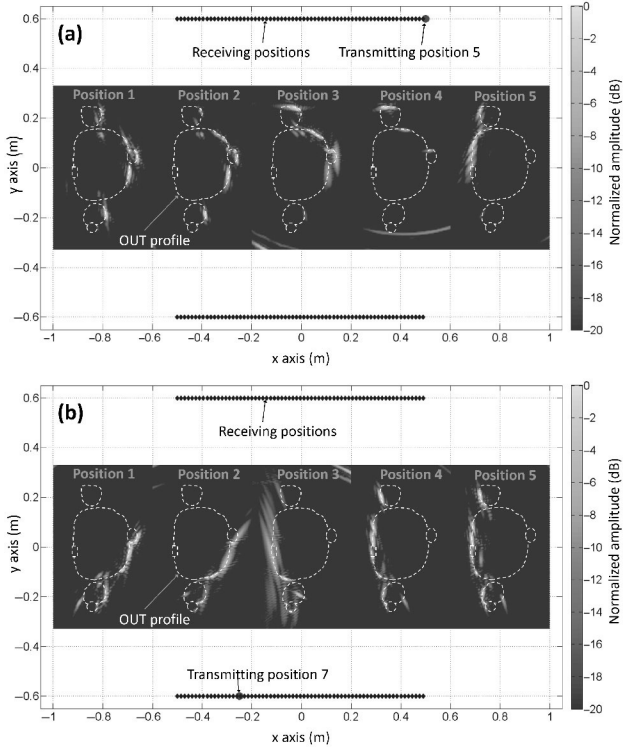
Fig. 2. 2-D example layout. OUT is displaced from position $x = -0.8$ m to $x = +0.8$ m, in five steps ($N_{pos} = 5$). 5 Tx and 50 Rx per side are considered.

panel of receivers, thus resulting in $N_{tx} = 10$ transmitters. The
 described layout is plotted in Fig. 2. The essential aspect is that,
 in order to image the entire body surface, for every transmitter,
 receivers on both walls must receive the scattered waves (not
 just those adjacent to a given transmitter.)

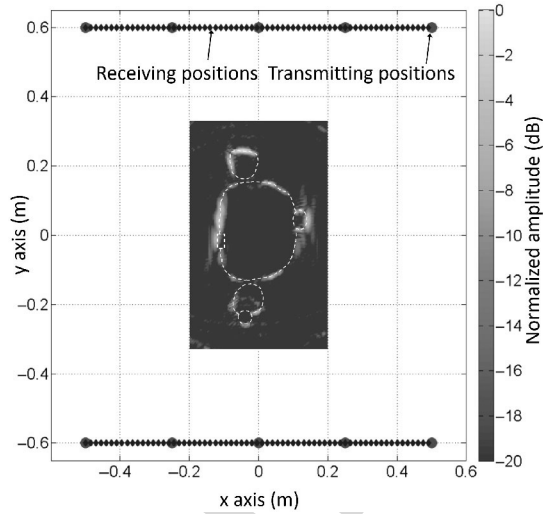
The object under test (OUT) models the cross section of
 a human body torso (for a more realistic simulation, arms,
 and waist are not connected), with three attached objects on
 it represented as protrusions on the front, back, and arm. The
 object in the front is an elliptical cross-sectional metallic object.
 Dielectric objects ($\epsilon_r = 3.5$) are placed on the back (square
 cross section) and on the right arm. The OUT is displaced
 from the position $x = -0.8$ m to $x = 0.8$ m in 40-cm steps
 obtaining $N_{pos} = 5$ intermediate positions. For every position,
 the ten transmitters are sequentially activated and the scattered
 field is collected in the receiving points. A realistic composi-
 tion of the human body tissue is considered [16], using a
 finite-difference frequency-domain (FDFD) code [17], [18] to
 calculate the scattered field for every transmitter and every
 position. FDFD simulation results have confirmed that, due to
 the high conductivity of the skin in the frequency band of inter-
 est, the assumption that the OUT is a perfect electric conductor
 (PEC) is a good approximation for most cases.

The data are then used to create one reflectivity image for
 each intermediate position, ρ^p according to (1) and (2). The
 imaging domain is an $(X, Y) = (0.4, 0.6)$ m rectangle, dis-
 cretized in 81×121 pixels and centered in (x'_p, y'_p, z'_p) . In this
 case, the computational cost is low and the image is recovered
 using the standard backpropagation algorithm in (1). For every p th
 OUT position and t th active transmitter, the image is recovered
 in about 1 s using a conventional laptop (2.5-GHZ CPU and 4-
 GB RAM memory). As the 2-D imaging code is not parallelized
 yet, it takes about 50 s for the entire reconstruction.

The obtained images for two different active transmitters
 when the OUT is in each of the intermediate positions are pre-
 sented in Fig. 3. It is clear that each transmitter allows the
 reconstruction of different areas of the body depending on its
 relative position inside the imaging system. The image obtained
 for the central position, combining the images created using all
 the transmitters according to (2), is presented in Fig. 4.



F3:1 Fig. 3. Obtained images (normalized reflectivity amplitude in dB) for two dif-
 F3:2 ferent active transmitters and five intermediate positions using the setup in
 F3:3 Fig. 2. Active transmitters are depicted as red points. Blue points represent
 F3:4 receivers positions.



F4:1 Fig. 4. Obtained image when the OUT is in the central position and the image
 F4:2 is created using all transmitters according to (2).

226 The reflectivity image created by the system at each position
 227 is obtained as

$$I(x'', y'', z'') = \sum_{p=1}^{N_{pos}} |\rho(x' - x'_p, y' - y'_p, z' - z'_p)| \quad (3)$$

228 where the reflectivity of all the positions is centered at the origin
 229 of coordinates before being combined. Absolute value is used
 230 since the position of the OUT relative to the imaging system can
 231 slightly change from position to position, which prevents the

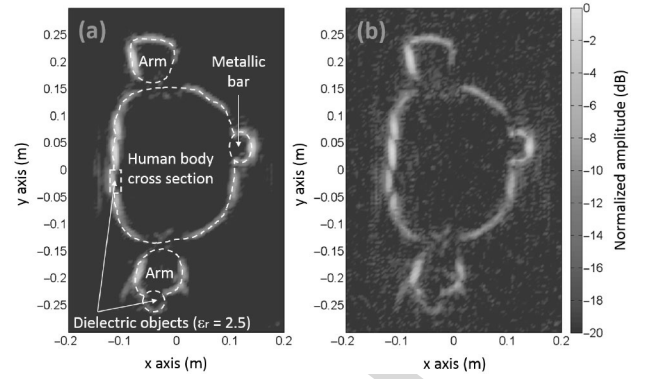


Fig. 5. Recovered OUT profile when combining in amplitude the five images F5:1
 (one for each position). (a) SNR = 10 dB. (b) SNR = -20 dB. F5:2

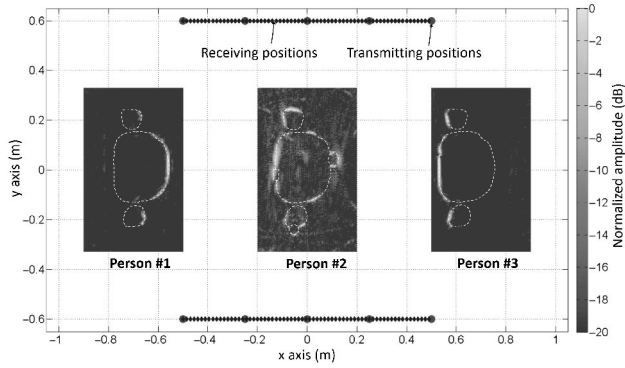
combination of the images of each position in amplitude and 232
 and phase. Fig. 5 presents the final result when the five analyzed 233
 positions are combined according to (3), and when the object 234
 retains exactly the same configuration for all positions and it is 235
 only displaced in the x direction. This proves the ability of the 236
 proposed system to obtain a complete contour reconstruction. 237
 In general, the images used for threat detection in a final 238
 configuration would be the ones generated in each position as the 239
 one in Fig. 4. 240

Combining the information from multiple transmitters and 241
 positions also helps to increase the dynamic range of the system. 242
 Sensitivity analysis has been performed: first, the recorded 243
 signal strength in the receiving arrays for every transmitting element 244
 and OUT position has been evaluated. The case in which maximum 245
 power is recorded corresponds to the OUT at the central position 246
 illuminated by the center transmitters. The minimum power levels 247
 are recorded for the OUT in positions 1 or 248
 5 illuminated by the closest pair of transmitters, as only a small 249
 fraction of the scattered field is collected by the arrays. The 250
 received power difference between these two cases is 11 dB. 251

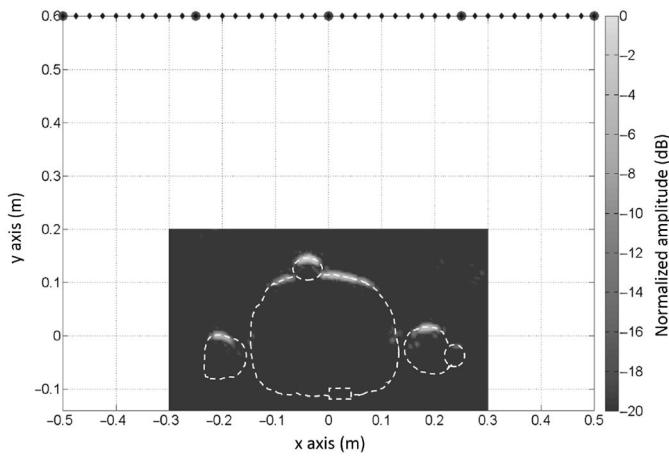
Next, noise has been added to the field samples according to 252
 different signal-to-noise ratio (SNR) levels relative to the maximum- 253
 recorded power case. Figs. 3–5(a) correspond to SNR = 10 dB, and 254
 Fig. 5(b) to SNR = -20 dB. Thanks to the combination of multiple 255
 OUT positions and incident directions, the resulting mm-wave imaging 256
 system is able to work with low SNR. 257
 258

The capability of imaging multiple users within the hallway 259
 has been also evaluated. For this purpose, the OUT placed at the 260
 center position (as in Fig. 4) is considered, but with two more 261
 OUTs (with no attached objects) at $x = 0.7$ and $x = -0.7$ m, a 262
 scenario that could correspond to a high passenger throughput 263
 situation. Due to the use of FDFD simulations, multiple 264
 reflections among OUTs are considered. Results are depicted in 265
 Fig. 6. It can be noticed that, with respect to Fig. 4, the center 266
 OUT is worse imaged due to the multipath effects. It is also 267
 possible to create the image of the front and the back of the 268
 OUTs placed at $x = 0.7$ and $x = -0.7$ m, and these results are 269
 not affected by multipath as much as the center OUT. 270

In order to compare this work with current state of the art 271
 systems, Fig. 7 presents the obtained image when the same con- 272
 tour is facing a line containing the transmitters and receivers. In 273



F6:1 Fig. 6. Recovered image for three OUTs placed at the same time in the hallway.
 F6:2 The image is created by combining all transmitters according to (2).



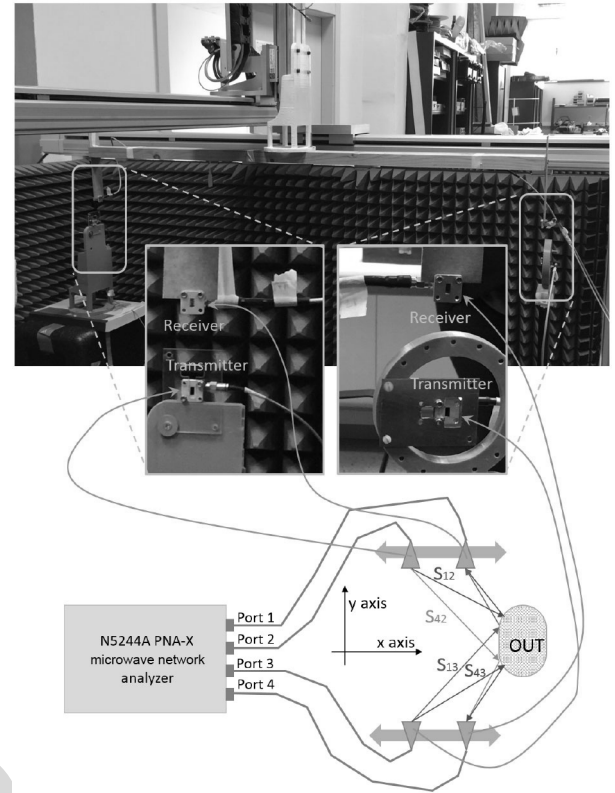
F7:1 Fig. 7. Obtained image using state-of-the-art configurations where transmitters
 F7:2 and receivers are placed in the same aperture and facing the person under test.
 F7:3 The image is generated combining the five transmitters according to (2).

274 this case, different areas of the front of the contour cannot be
 275 recovered and the area that is reconstructed is much smaller
 276 than the one of Fig. 4. Concerning detection capabilities, note
 277 that the dielectric object placed on the arm is hardly detected
 278 in Fig. 7 as the energy is not scattered back to the receiving
 279 array. In the case of the on-the-move system, it can be better
 280 detected (see Figs. 4 and 5), as it is possible to find a configura-
 281 tion along the conveyor belt in which the energy is reflected
 282 in the dielectric-skin transition, then backscattered to one of the
 283 receiving arrays.

284 This 2-D example proves that, in the proposed on-the-move
 285 layout, the fact that some of the transmitters and receivers are
 286 separated with a subtended angle relative to the person equal or
 287 greater than 90° provides information from all possible wave
 288 incident angles.

289 V. VALIDATION WITH MEASUREMENTS

290 The proposed on-the-move imaging concept has been validated with measurements. Ka frequency band (26.5–40 GHz)
 291 has been selected to avoid hardware switching between different frequency bands. In order to ensure the maximum illumination within the hallway, WR-28 open-ended waveguides are selected as antennas.
 292
 293
 294
 295

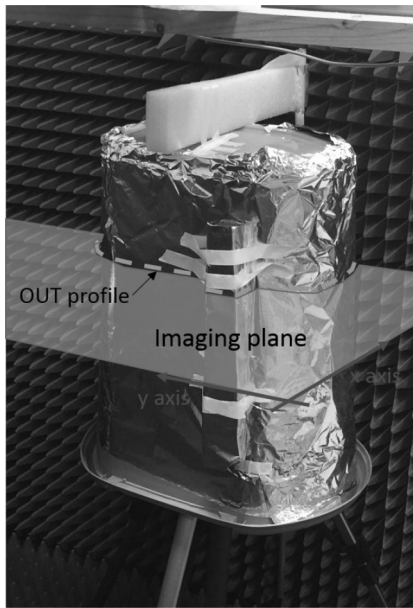


F8:1 Fig. 8. Ka-band measurement system for on-the-move concept experimental
 F8:2 validation. WR-28 open-ended waveguides are connected to the vector network
 F8:3 analyzer ports. Receivers are mounted on a three-axis positioner.

The setup is mounted on an XYZ table measurement range [19], so some mechanical restrictions apply to the placement of the OUT, transmitters, and receiving positions (Fig. 8). In order to take advantage of the whole span of the XYZ measurement range, scattered field samples are collected in 161 points ranging from $x = -0.6$ m to $x = 0.6$ m, placed at $Y_0 = 0$ m and $Y_0 = 1.3$ m. Five transmitting positions are interleaved among the receivers, thus resulting in $N_{tx} = 10$ transmitting positions. Transmitters and receivers are separated 5 cm in height. Horizontal polarization is considered to reduce coupling between transmitter and receiver. The imaging setup is depicted in Fig. 8: two transmitters and two receivers are connected to the ports of a vector network analyzer. The power reference level is 0 dBm for all the ports. For every receiving position along the x-axis, four S-parameters are measured, as shown in Fig. 8, corresponding to the combination of each transmitter with both receivers.

The positioner of the XYZ table is used to move the receivers from each side of the hallway at the same time, as shown in Fig. 8. The pair of transmitters is manually placed at five positions along the x-axis, using the XYZ positioner as reference. For every pair of transmitting positions, acquisition time takes 3 min, and therefore, overall acquisition time for every OUT position is 15 min.

The OUT, shown in Fig. 9, is an aluminum foil-covered plastic bin with a metallic bar attached to one of the sides. Due to its translation symmetry in z-axis, it allows for 2-D analysis in an XY plane placed at $(z = h_{tx} + h_{rx}/2)$, where h_{tx} is the



F9:1 Fig. 9. Photograph of the OUT imaged with the proposed experimental setup.
 F9:2 Receivers are mounted on a three-axis positioner.

324 height of the transmitters, and h_{rx} the height of the receivers.
 325 As mentioned in Section II, using metal to simulate the human
 326 body skin in the Ka band is an acceptable approach due to the
 327 high conductivity of the skin in mm-wave frequency bands [16].
 328 Three positions of the OUT were considered.

329 The same data processing as in Section III has been applied.
 330 The image obtained for every position, combining the images
 331 created using all the transmitters according to (2), is depicted in
 332 Fig. 10(a). It can be noticed that, for positions 1 and 3, the front
 333 and the back of the OUT are imaged, and the sides of the OUT
 334 are visible for position 2.

335 Fig. 10(b) presents the final result combining the three OUT
 336 positions according to (3), where the OUT profile can be
 337 observed. In this case, combination is done taking the displace-
 338 ment of each individual image with respect to the center of the
 339 imaging domain. In practical, combination of the radar images
 340 for different positions of the person in the hallway can be based
 341 on video frames, linking video, and radar images.

342 In addition to the presented results, the measurement setup
 343 has been simulated, aiming to evaluate the correspondence
 344 between simulations and measurements. Results for position 2
 345 are compared in Fig. 11. Good agreement between the recon-
 346 structed parts of the OUT for simulations and measurements is
 347 obtained.

VI. 3-D CONFIGURATION

348
 349 Next, the extension from 2-D to 3-D is presented. The layout
 350 of the proposed on-the-move 3-D system is presented in Fig. 12.
 351 The setup is composed of multiple synchronized transmitters
 352 and receivers. Lateral receiving apertures of size $(X, Z) =$
 353 $(1, 2)$ m, are placed at $Y_0 = 0.75$ m. The size of the panels is
 354 chosen to provide an approximated cross-range resolution of
 355 1 cm along the z-axis and 2 cm in the x-axis.

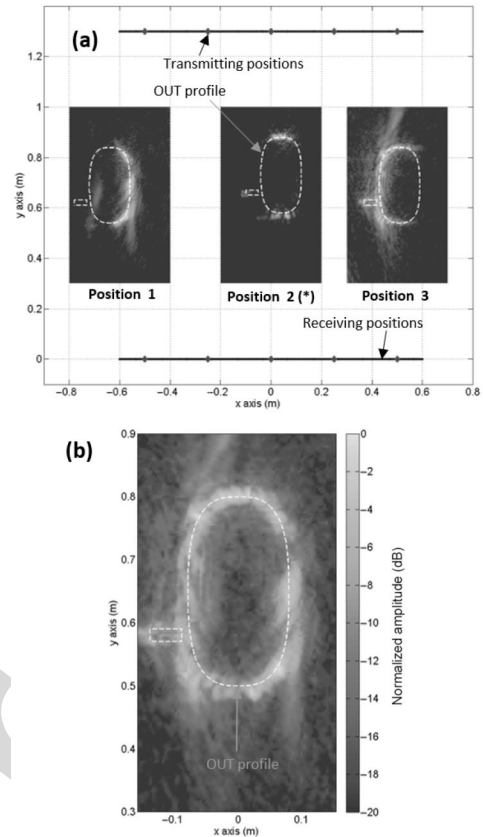


Fig. 10. Recovered OUT profile. (a) Image created on every position using
 all the transmitters according to (2). In the case of position 2, only the
 center transmitting positions ($x_{inc}^t = 0$ m) were available. (b) OUT profile when
 combining in amplitude the three images of (a).

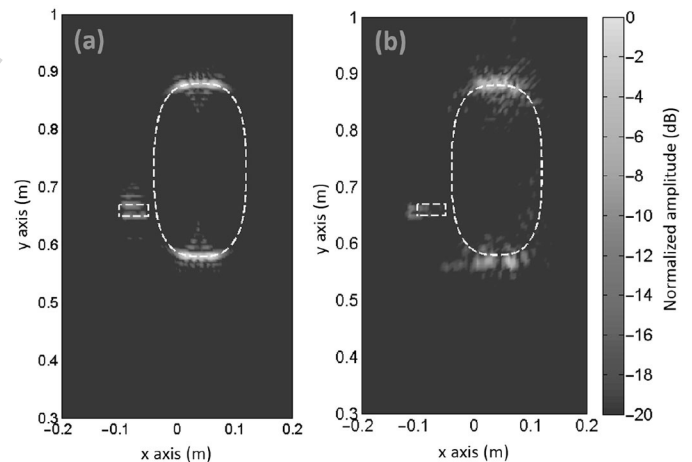


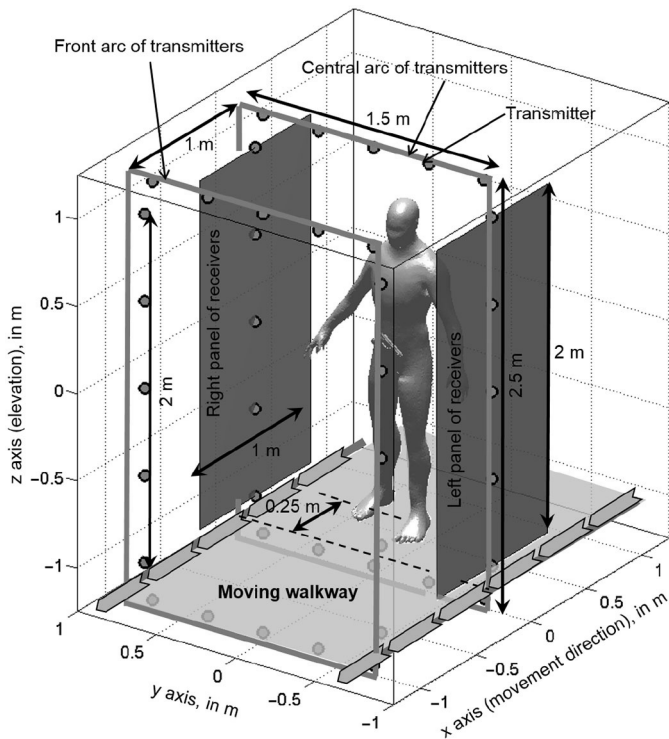
Fig. 11. Recovered OUT profile, position 2 (with center transmitting posi-
 tions). (a) From simulated data. (b) From measurements.

For this preliminary setup, Nyquist sampling requirements
 are considered for the receiving panels, thus acquiring the field
 in 201×401 receiving positions per panel. Subsampling tech-
 niques as presented in [2] and [5] combined with a modified
 FFT algorithm for multistatic imaging with subsampled arrays
 can be efficiently applied in this setup to reduce the number
 of receivers in more than 90% [2], although this analysis is
 beyond the scope of this contribution. A 15-GHz bandwidth

F10:1
 F10:2
 F10:3
 F10:4

F11:1
 F11:2

356
 357
 358
 359
 360
 361
 362
 363



F12:1 Fig. 12. Layout of the mm-wave scanner for personnel screening. For the sake of
 F12:2 simplicity, just two arcs of transmitters, at $x = 0$ m, and $x = -1$ m,
 F12:3 are considered. The person under test is placed at $x = 0.25$ m.

364 (BW), from 15 to 30 GHz, is chosen, similarly to the UWB
 365 imaging system described in [5]. This BW provides an approx-
 366 imate range resolution of 1 cm, although, for near-field radar
 367 imaging, besides the frequency and aperture size, the final system
 368 lateral and range resolutions are given by (2) and (3) of
 369 [20], respectively.

370 Hallway scanner dimensions have been selected to provide
 371 a resolution similar to other mm-wave scanners, as shown in
 372 Table I. It must be reminded that the number of receiving
 373 elements can be reduced in the hallway system.

374 Concerning processing time, the fastest operational mm-
 375 wave imaging systems listed in Table I are capable to provide
 376 detection results in less than 5 s, so the scanning process can
 377 take up to 10 s taking into account that the person needs to be
 378 placed in a particular position within the scanner. For the pre-
 379 sented system, the overall scanning process would be limited
 380 by the time the person needs to go through the hallway.

381 Three arcs of transmitters, centered at $x = +1$, 0, and -1 m,
 382 and each having 20 elements evenly spaced along y - and z -axes,
 383 are considered. For the sake of simplicity, only the ones at -1
 384 and 0 m, depicted in Fig. 12, will be considered to obtain the
 385 results in this section. Some of the transmitters are placed on top
 386 and below the body to ensure the areas with larger curvature (as
 387 the top of the chest and shoulders) are reconstructed.

388 A physical optics (PO) code [21], [22] in combination with a
 389 visibility algorithm [23] has been used to predict the parts of the
 390 body model in Fig. 12 that are illuminated by every transmitter.
 391 Also, PO provides the amount of scattered field collected on the
 392 panels. Thus, it is possible to evaluate if a certain layout
 393 of transmitters is capable of illuminating the entire person after
 394 crossing the hallway and to estimate the field scattered by the

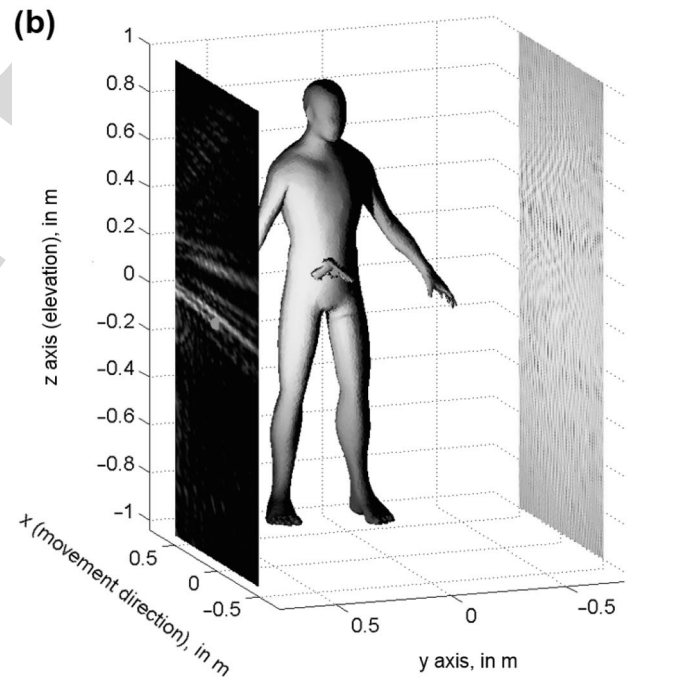
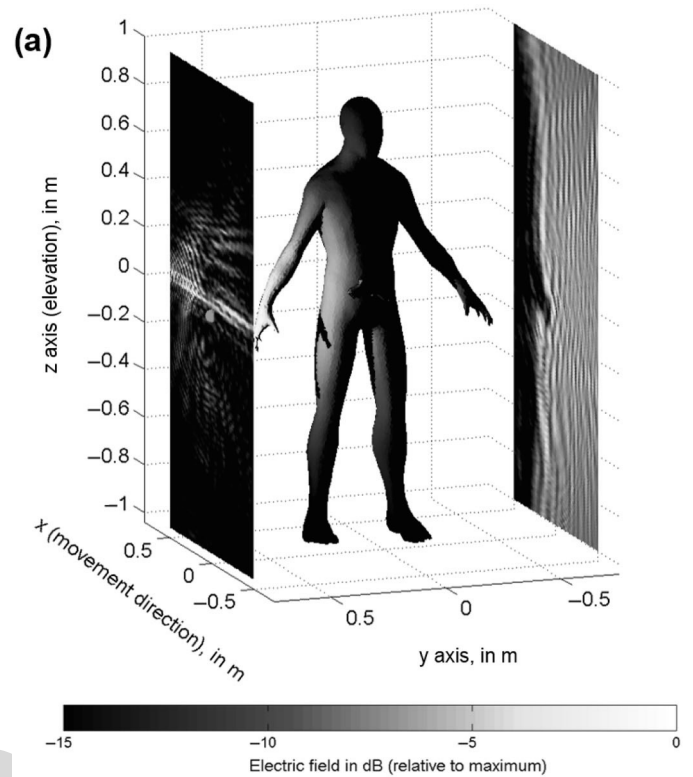
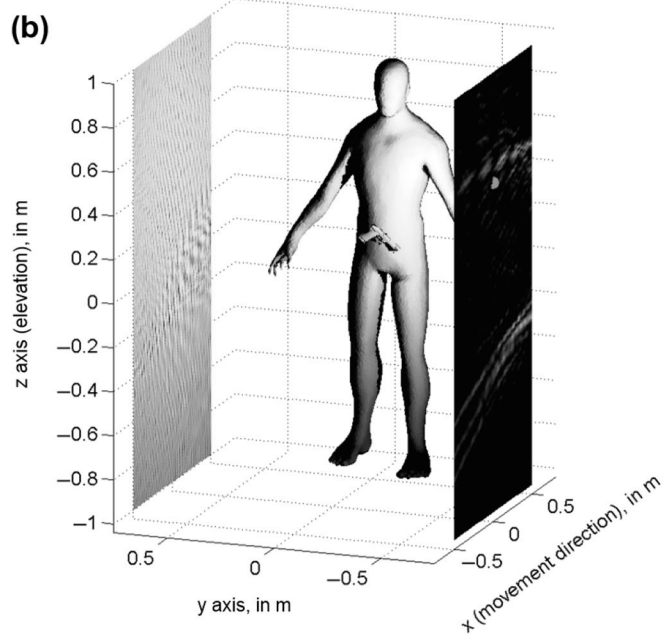
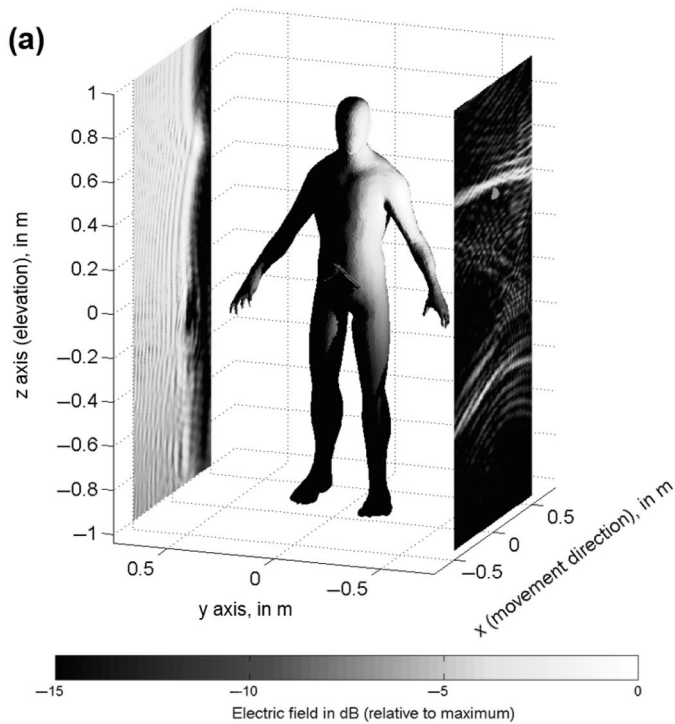


Fig. 13. Examples of human body illumination using one transmitter (high- F13:1
 F13:2 lighted in green) and scattered field on the array panels when the body model is
 F13:3 centered in (a) 0.25 m and (b) 0.75 m.

illuminated areas on the receiving panels. For these simulations, 395
 the human body is assumed to behave as a PEC in the 15–30- 396
 GHz frequency band. 397

As an example, Figs. 13 and 14 show the regions of the 398
 human body under test illuminated by two different transmitters, 399
 as well as the field received on the lateral panels. Note that, 400
 even for a single position of the person in the hallway, different 401



F14:1 Fig. 14. Examples of human body illumination using one transmitter (high-
 F14:2 lighted in green) and scattered field on the array panels when the body model is
 F14:3 centered in (a) 0.25 m and (b) 0.75 m.

402 areas of the body are illuminated. This layout increases the
 403 amount of information thanks to the spatial diversity of the
 404 multistatic illumination.

405 Regarding the inverse method to create images in this system and due to the large computational cost for the imaging,
 406 when the backpropagation is implemented in 3-D, the above-
 407 mentioned Fourier-based technique for multistatic imaging [9]
 408 has been used. The efficient use of fast Fourier transforms
 409 (FFT) provides 3-D whole body imaging in almost real time
 410 using conventional hardware.
 411

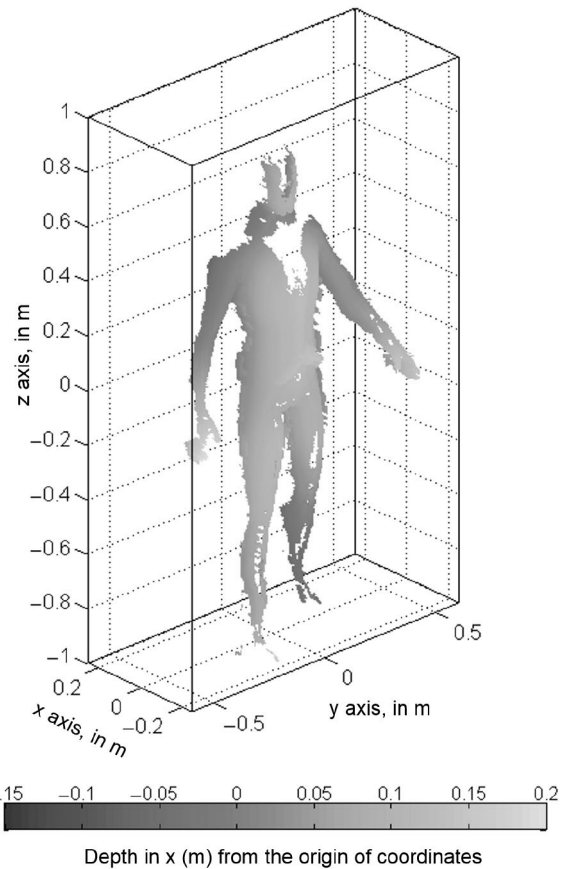
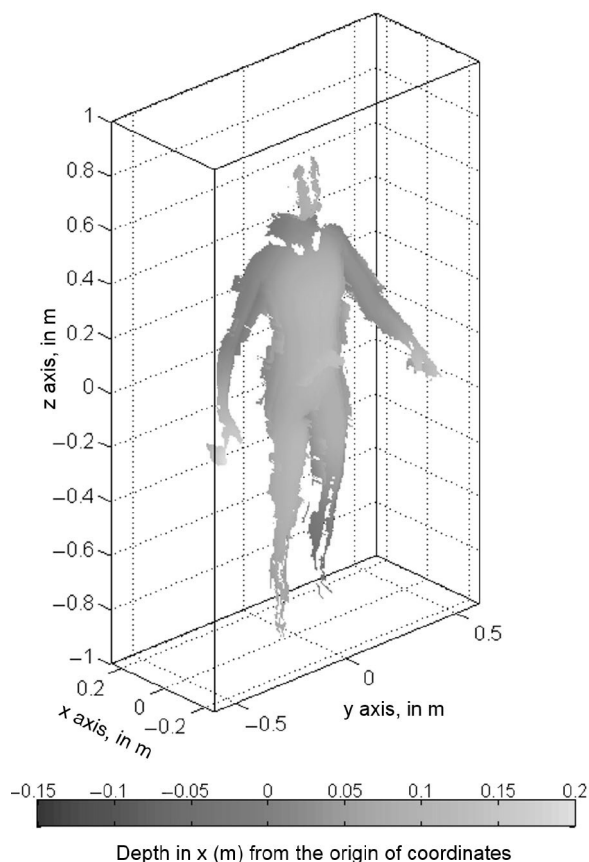


Fig. 15. Person placed at $x = 0.25$ m. Recovered human body and concealed
 object geometry from backpropagation imaging. F15:1 F15:2

As an application example to show the performance of the
 proposed configuration, an OUT consisting on a person carrying
 a concealed weapon in the belt has been considered. For
 the sake of simplicity, only two positions are analyzed: person
 standing at $x = 0.25$ m and at $x = 0.75$ m. In this example,
 the goal is to clearly illustrate the different nature of the multistatic
 information collected on each position, rather than a rigorous
 reconstruction of the whole body.

For every position, transmitter, and receiving panel, the
 amount of data to be processed is: 201×401 spatial samples \times
 121 frequency samples ($= 9.75 \times 10^6$ scattered field samples),
 which also determines the number of imaging points in the
 case of Fourier-based imaging [9]. A workstation with 32 cores
 at 2.1 GHz and 128-GB RAM was used for data processing.
 Overall calculation time for every transmitter was 30 s (1200 s
 total for the 40 used transmitters). The processing has been
 done using a sequential Matlab code and has not been optimized
 for real time imaging yet.

Imaging results are depicted in Figs. 15 and 16, correspond-
 ing to the person's placement at $x = 0.25$ m and $x = 0.75$ m,
 respectively. Reflectivity points above -25 dB with respect to
 the maximum are coded in depth according to x-axis, allowing
 the recovery of the human body profile and potential concealed
 weapons. Comparison of Figs. 15 and 16 provides a clear exam-
 ple of the on-the-move imaging concept effectiveness. In the
 case of Fig. 15 (person placed at $x = 0.25$ m), the human body
 sides and some areas of the chest are imaged by the system. In



F16:1 Fig. 16. Person placed at $x = 0.75$ m. Recovered human body and concealed
 F16:2 object geometry from backpropagation imaging.

439 Fig. 16 (person placed at $x = 0.75$ m), the top of the chest and
 440 the shoulders are recovered.

441 In the final system, multiple images, as the two presented
 442 examples, can be created and analyzed at video rate to detect
 443 any possible threats. Algorithms for mesh generation and auto-
 444 matic thread detection, such as the one used in [8], can be
 445 applied.

VII. CONCLUSION

447 This work presented a novel concept for personnel scanning
 448 in airports and other checkpoints. Unlike the current imaging
 449 systems, the proposed system allows for continuous movement
 450 of the subject while being scanned; this will greatly increase
 451 the system throughput when compared with state-of-the-art sys-
 452 tems. This improvement is possible thanks to the use of a fully
 453 multistatic radar configuration, where some of the transmitters
 454 and receivers are separated with a subtended angle relative to
 455 the person greater than 90 degrees to capture information from
 456 all possible wave incident angles. In this way, the system is
 457 able to create a complete contour reconstruction as the person
 458 moves inside the system. The use of a small number of trans-
 459 mitters allows for fast image creation as all the transmitters can
 460 be sequentially activated in a short amount of time. 2-D and 3-D
 461 simulation-based results confirm the good imaging capabilities
 462 of the proposed system; 2-D results have also been validated
 463 using measurements. Further work will be related with the setup

optimization, including the use of sparse arrays and other tech- 464
 niques to reduce the number of receivers, and with experimental 465
 validation. 466

REFERENCES

- 467
- [1] IATA. *Checkpoint of the Future. Executive Summary* [Online]. Available: 468
<http://www.iata.org/whatwedo/security/Documents/cof-executive-> 469
[summary.pdf](http://www.iata.org/whatwedo/security/Documents/cof-executive-), accessed on Mar. 16, 2015. 470Q2
 - [2] S. S. Ahmed, A. Schiessl, F. Gumbmann, M. Tiebout, S. Methfessel, 471
 and L. Schmidt, "Advanced microwave imaging," *IEEE Microw. Mag.*, 472
 vol. 13, no. 6, pp. 26–43, Sep./Oct. 2012. 473
 - [3] S. S. Ahmed, "Personnel screening with advanced multistatic imaging 474
 technology," in *Proc. SPIE Defense Secur. Sens.*, 2013, p. 87150B. 475
 - [4] D. Sheen, D. McMakin, and T. Hall, "Three-dimensional millimeter-wave 476
 imaging for concealed weapon detection," *IEEE Trans. Microw. Theory* 477
Techn., vol. 49, no. 9, pp. 1581–1592, Sep. 2001. 478
 - [5] X. Zhuge and A. Yarovoy, "A sparse aperture MIMO-SAR-based UWB 479
 imaging system for concealed weapon detection," *IEEE Trans. Geosci.* 480
Remote Sens., vol. 49, no. 1, pp. 509–518, Jan. 2011. 481
 - [6] D. M. Sheen, D. L. McMakin, and T. E. Hall, "Combined illumination 482
 cylindrical millimeter-wave imaging technique for concealed weapon 483
 detection," in *Proc. AeroSense*, 2000, pp. 52–60. 484
 - [7] Y. Rodríguez-Vaqueiro, Y. Álvarez López, B. Gonzalez-Valdes, 485
 J. A. Martinez, F. Las-Heras, and C. M. Rappaport, "On the use of 486
 compressed sensing techniques for improving multistatic millimeter- 487
 wave portal-based personnel screening," *IEEE Trans. Antennas Propag.*, 488
 vol. 62, no. 1, pp. 494–499, Jan. 2014. 489
 - [8] B. Gonzalez-Valdes, Y. Alvarez-Lopez, J. A. Martinez-Lorenzo, F. Las 490
 Heras Andres, and C. M. Rappaport, "On the use of improved imag- 491
 ing techniques for the development of a multistatic three-dimensional 492
 millimeter-wave portal for personnel screening," *Prog. Electromagn.* 493
Res., vol. 138, pp. 83–98, 2013. 494
 - [9] Y. Alvarez *et al.*, "Fourier-based imaging for multistatic radar systems," 495
IEEE Trans. Microw. Theory Techn., vol. 62, no. 8, pp. 1798–1810, Aug. 496
 2014. 497
 - [10] G. Yates, A. Horne, A. Blake, and R. Middleton, "Bistatic SAR image 498
 formation," *Inst. Elect. Eng. Proc. Radar Sonar Navigat.*, vol. 153, no. 3, 499
 pp. 208–213, Jun. 2006. 500
 - [11] R. Burkholder, I. Gupta, and J. Johnson, "Comparison of monostatic and 501
 bistatic radar images," *IEEE Trans. Antennas Propag. Mag.*, vol. 45, no. 3, 502
 pp. 41–50, Jun. 2003. 503
 - [12] B. Gonzalez-Valdes, C. Rappaport, and J. A. Lorenzo-Martinez, "On- 504
 the-move active millimeter wave interrogation system using a hallway 505
 of multiple transmitters and receivers," in *Proc. IEEE Antennas Propag.* 506
Soc. Int. Symp. (APSURSI), 2014, pp. 1107–1108. 507
 - [13] B. Gonzalez-Valdes, C. Rappaport, and J. Martinez-Lorenzo, "On the 508
 move millimeter wave interrogation system with a hallway of multiple 509
 transmitters and receivers," U.S. Patent 14 562 094, Dec. 5, 2014. 510
 - [14] M. Soumekh, "Bistatic synthetic aperture radar inversion with application 511
 in dynamic object imaging," *IEEE Trans. Signal Process.*, vol. 39, no. 9, 512
 pp. 2044–2055, Sep. 1991. 513
 - [15] Y. Alvarez, J. Martinez, F. Las-Heras, and C. Rappaport, "An inverse 514
 fast multipole method for imaging applications," *IEEE Antennas Wireless* 515
Propag. Lett., vol. 10, pp. 1259–1262, Nov. 2011. 516
 - [16] D. Andreuccetti, R. Fossi, and C. Petrucci, "An Internet resource for the 517
 calculation of the dielectric properties of body tissues in the frequency 518
 range 10 Hz–100 GHz," Internet document, 1997 [Online]. Available: 519
<http://niremf.ifac.cnr.it/tissprop/>, accessed on Sep. 15, 2015, IFAC-CNR, 520
 Florence, Italy, 1997, based on data published by C. Gabriel *et al.* in 1996. 521
 - [17] A. W. Morgenthaler and C. M. Rappaport, "Scattering from lossy dielec- 522
 tric objects buried beneath randomly rough ground: Validating the semi- 523
 analytic mode matching algorithm with 2-D FDFD," *IEEE Trans. Geosci.* 524
Remote Sens., vol. 39, no. 11, pp. 2421–2428, Nov. 2001. 525
 - [18] C. M. Rappaport, Q. Dong, E. Bishop, A. Morgenthaler, and 526
 M. E. Kilmer, "Finite difference frequency domain (FDFD) modeling of 527
 two dimensional TE wave propagation," in *Proc. URSI Symp. Conf.*, Pisa, 528
 Italy, 2004. 529Q3
 - [19] A. Arboleya, Y. Alvarez, and F. Las-Heras, "Millimeter and submillimeter 530
 planar measurement setup," in *Proc. IEEE Antennas Propag. Soc. Int.* 531
Symp. (APSURSI), 2013, pp. 1–2. 532
 - [20] S. S. Ahmed, A. Schiessl, and L.-P. Schmidt, "A novel active real-time 533
 digital-beamforming imager for personnel screening," in *Proc. 9th Eur.* 534
Conf. Synth. Aperture Radar (EUSAR), Apr. 2012, pp. 178–181. 535

- 536 [21] J. Meana, J. Martinez-Lorenzo, F. Las-Heras, and C. Rappaport, "Wave
537 scattering by dielectric and lossy materials using the modified equivalent
538 current approximation (MECA)," *IEEE Trans. Antennas Propag.*, vol. 58,
539 no. 11, pp. 3757–3761, Nov. 2010.
- 540 [22] L. E. Tirado, J. A. Martinez-Lorenzo, B. Gonzalez-Valdes, C. Rappaport,
541 O. Rubinos-Lopez, and H. Gomez-Sousa, "GPU implementation of
542 the modified equivalent current approximation (MECA) method," *Appl.*
543 *Comput. Electromagn. Soc. J.*, no. 9, Sep. 2012.
- 544 [23] J. Gutiérrez Meana, F. L. Las Heras Andrés, and J. Á. Martínez Lorenzo,
545 "A comparison among fast visibility algorithms applied to computational
546 electromagnetics," *Appl. Comput. Electromagn. Soc. J.*, 2009.



Borja Gonzalez-Valdes (M'xx) received the B.S. and Ph.D. degrees in electrical engineering from the University of Vigo, Vigo, Spain, in 2006 and 2010, respectively.

From 2006 to 2010, he was with the Antenna and Optical Communications Group, University of Vigo. From 2008 to 2009, he was a Visiting Researcher with the Gordon Center for Subsurface Sensing & Imaging Systems, Northeastern University, Boston, MA, USA. In 2011, he joined the Awareness and

Localization of Explosives-Related Threats Center of Excellence, Northeastern University. Since 2015, he has been a Postdoctoral Researcher affiliated with the AtlantTIC Research Center, University of Vigo. His research interests include antenna design, inverse scattering, radar, advanced imaging techniques, and THz technology.



Yuri Álvarez (S'06–M'09–SM'15) was born in Langreo, Spain, in 1983. He received the M.S. and Ph.D. degrees in telecommunication engineering from the University of Oviedo, Gijn, Spain, in 2006 and 2009, respectively.

He was a Visiting Scholar at the Department of Electrical Engineering and Computer Science, Syracuse University, Syracuse, NY, USA, in 2006 and 2008; a Visiting Postdoc at the Gordon Center for Subsurface Sensing and Imaging Systems (CenSSIS)ALERT (Awareness and Localization of

Explosive Related Threats) Center of Excellence, Northeastern University, Boston, MA, USA, from 2011 to 2014; and a Visiting Postdoc at ELEDIA Research Center, Trento, Italy, in 2015. He is currently an Assistant Professor with the Signal Theory and Communications, University of Oviedo, Gijn, Spain. His research interests include antenna diagnostics, antenna measurement techniques, RF techniques for indoor location, inverse scattering and imaging techniques, and phaseless methods for antenna diagnostics and imaging.

Dr. Alvarez was the recipient of the 2011 Regional and National Awards to the Best Ph.D. Thesis on Telecommunication Engineering (category: security and defense).



Yolanda Rodriguez-Vaqueiro (S'xx) received the B.S. and M.S. degrees in electrical engineering from the University of Vigo, Vigo, Spain, in 2009, and the Ph.D. degree in electrical engineering from Northeastern University, Boston, MA, USA, in 2015 (after defending her thesis: Compressive Sensing for Electromagnetic Imaging Using a Nesterov-Based Algorithm).

She is a Postdoctoral Researcher affiliated with the AtlantTIC Research Center, University of Vigo. In 2011, she obtained a Research Assistant grant from the ALERT (Awareness and Localization of Explosive Related Threats) Center of Excellence, Northeastern University. She was also granted as a Junior Researcher with the University of Vigo.

Dr. Rodriguez-Vaqueiro was the recipient of the Research-Impact Award by the Department of Electrical and Computer Engineering, Northeastern University (for her work during the Ph.D. studies), the Best Paper Award in the 2012 IEEE Homeland Security Conference, Honorable Mention in the 2012 Student Paper Competition in the 2013 IEEE APS/URSI Conference, the Best Paper Award in the 2014 European Conference on Antennas and Propagation, the Burke/Yannas Award to the most original research study in the field of bioengineering in the 2015 American Burn Association (ABA) Meeting, and the Research-Impact Award by the Department of Electrical and Computer Engineering, Northeastern University, in May 2015.



Ana Arboleya-Arboleya received the M.Sc. degree in telecommunication engineering from the University of Oviedo, Oviedo, Spain, in 2009, where she is currently pursuing the Ph.D. degree in telecommunication engineering. Since 2008, she has been a Research Assistant within the Signal Theory and Communications Research Group, TSC-UNIOVI, Department of Electrical Engineering, University of Oviedo. She was a Visiting Scholar in 2014 and 2015 at the Department of Radio Science and Engineering and MilliLab, Aalto University, Espoo, Finland. Her research interests include antenna diagnostics and measurement systems and techniques and high-frequency imaging techniques and applications.



Antonio García-Pino (S'87–M'89–SM'05) was born in Valdemoro, Madrid, Spain, in 1962. He received the M.S. and Ph.D. degrees in telecommunications engineering from the Polytechnic University of Madrid (UPM), Madrid, Spain, in 1985 and 1989, respectively.

From 1985 to 1989, he was a Research Assistant with the Radiation Group, UPM. He joined as an Associate Professor with the Department of Technologies of Communications, University of Vigo, Vigo, Spain, in 1989, becoming Full Professor

in 1994. In 1993, he was a Visiting Researcher at the Center for Electromagnetics Research, Northeastern University, Boston, MA, USA. From 2006 to 2010, he was the Vice-Rector of Academic Organization and Faculty, and currently, he is the Director of the International Doctoral School, both at University of Vigo. His research interests include shaped-reflector antennas for communication and radar applications, high-frequency backscattering, computational electromagnetics, and THz technology. In these topics, he has authored more than 100 technical papers in journal and conferences and he has been an advisor of 14 Ph.D. thesis.



Carey M. Rappaport (SM'96–F'06) received the S.B. degree in mathematics, the S.B., S.M., and E.E. degrees in electrical engineering in 1982, and the Ph.D. degree in electrical engineering in 1987 from the Massachusetts Institute of Technology (MIT), Cambridge, MA, USA.

He was a Teaching and Research Assistant with MIT from 1981 until 1987, and during the summers at COMSAT Labs, Clarksburg, MD, USA, and the Aerospace Corp., El Segundo, CA, USA.

He joined the faculty at Northeastern University, Boston, MA, USA, in 1987. He has been a Professor of Electrical and Computer Engineering since July 2000. In 2011, he was appointed as a College of Engineering Distinguished Professor. In fall 1995, he was a Visiting Professor of Electrical Engineering at the Electromagnetics Institute, Technical University of Denmark, Lyngby, Denmark, as part of the W. Fulbright International Scholar Program. In the second half of 2005, he was a Visiting Research Scientist at the Commonwealth Scientific Industrial and Research Organisation (CSIRO), Epping, Australia. He has consulted for CACI, Alion Science and Technology, Inc., Geo-Centers, Inc., PPG, Inc., and several municipalities on wave propagation and modeling, and microwave heating and safety. He was the Principal Investigator of an ARO-sponsored Multidisciplinary University Research Initiative on Humanitarian Demining, the Co-Principal Investigator of the NSF-sponsored Engineering Research Center for Subsurface Sensing and Imaging Systems (CenSSIS), and the Co-Principal Investigator and Deputy Director of the DHS-sponsored Awareness and Localization of Explosive Related Threats (ALERT) Center of Excellence. He has authored more than 400 technical journal and conference papers in the areas of microwave antenna design, electromagnetic wave propagation and scattering computation, and bioelectromagnetics, and has received two reflector antenna patents, two biomedical device patents, and four subsurface sensing device patents.

Prof. Rappaport is a member of Sigma Xi and Eta Kappa Nu professional honorary societies. He was the recipient of the IEEE Antenna and Propagation Society's H. A. Wheeler Award for the Best Applications Paper, as a Student in 1986.

607
608
609
610
611
612
613
614
615
616
617
618
619

620
621
622
623
624
625
626
627
628
629
630
631
632
633
634
635
636
637
638
639

640
641
642
643
644
645

646
647
648
649
650
651
652
653
654
655
656
657
658
659
660
661
662
663
664
665
666
667
668
669
670
671
672
673
674
675

676
677
678
679
680
681
682
683
684
685
686
687
688
689
690
691
692
693
694
695
696
697
698
699
700
701
702
703



Fernando Las-Heras (M'86–SM'08) received the M.S. and Ph.D. degrees in telecommunication engineering from the Technical University of Madrid (UPM), Madrid, Spain, in 1987 and 1990, respectively.

He was a National Graduate Research Fellow (1988–1990), and he held a position of Associate Professor with the Department of Signal, Systems, and Radiocommunications, UPM (1991–2000). From December 2003, he holds a Full Professor position with the University of Oviedo, Oviedo, Spain, where

he was the Vice-Dean for Telecommunication Engineering, Technical School of Engineering, Gijón, Spain (2004–2008). As of 2001, he was the Head of the Research Group Signal Theory and Communications TSC-UNIOVI, Department of Electrical Engineering, University of Oviedo. He was a Visiting Lecturer at the National University of Engineering, Rímac Lima, Peru, in 1996, a Visiting Researcher at Syracuse University, Syracuse, NY, USA, in 2000, and a short-term Visiting Lecturer at ESIGELEC, France, from 2005 to 2011. He held the Telefónica Chair on RF Technologies, ICTs applied to Environment and ICTs and Smartcities with the University of Oviedo (2005–2015). He has authored more than 300 articles published in academic journals and proceedings of international conferences, mainly in the areas of antenna design and the inverse electromagnetic problem with applications in diagnostic, measurement and synthesis of antennas, phaseless techniques, propagation, and microwave to THz imaging and localization, as well as in engineering education.

Dr. Las-Heras was a Member of the Board of Directors of the IEEE Spain Section (2012–2015), and from 2010, he was a Member of the Science, Technology, and Innovation Council of Asturias, Asturias, Spain.



Jose A. Martinez-Lorenzo (M'xx) received the B.S./M.S. degree in 2002 and the Ph.D. degree in 2005 from the University of Vigo, Vigo, Spain, both in electrical engineering.

He joined the faculty at University of Oviedo, Gijon, Spain, in 2004, where he was an Assistant Professor with the Department of Signal Theory and Communications. In 2006, he joined Bernard M. Gordon Center for Subsurface Sensing and Imaging Systems, Northeastern University, Boston, MA, USA. In 2010, he was a Research Assistant

Professor with the Department of ECE, Northeastern University. Since August 2013, he has been held a joint appointment with the Departments of MIE and ECE as a Tenure-Track Assistant Professor. He is an Active Member of Awareness and Localization of Explosives-Related Threats (ALERT) a DHS Center of Excellence awarded to Northeastern University. He has authored more than 140 technical journal and conference papers. His research interests include the understanding, modeling, and solving complex engineering problems, with an emphasis on mechanical and electromagnetic sensing and imaging methods for security and biomedical applications (i.e., explosive detection, breast cancer detection).

Prof. Martinez-Lorenzo has received funding from multiple agencies, including: DHS, DARPA, NSF, US Army, and the European Space Agency (ESA). He led the team that won the Best Paper Award in the 2012 IEEE Conference on Technologies for Homeland Security, for the paper on a compressed sensing approach for detection of explosive threats at standoff distances using a passive array of scatterers.

704
705
706
707
708
709
710
711
712
713
714
715
716
717
718
719
720
721
722
723
724
725
726
727
728
729
730

QUERIES

- Q1: Please provide captions for Fig. 3 subparts.
- Q2: Please provide year of publication for Ref. [1].
- Q3: Please provide page range for Refs. [18], [22], and [23].
- Q4: Please provide volume number for Ref. [22] and [23].
- Q5: Please provide the membership history (year) of the authors Borja Gonzalez-Valdes, Yolanda Rodriguez-Vaqueiro, and Jose A. Martinez-Lorenzo.
- Q6: Please provide year of completion for the S.B. degree in Mathematics, S.B., S.M. degrees in electrical engineering of author "Carey M. Rappaport."

IEEE PROOF